1-1-2016

C-Reactive Protein Interactions with Cellular Membranes and Supported Lipid Bilayers

Aml Abd Alhamed Alnaas
University of Denver

C-REACTIVE PROTEIN INTERACTIONS WITH CELLULAR MEMBRANES AND SUPPORTED LIPID BILAYERS

_____

A Dissertation

Presented to

the Faculty of Natural Sciences and Mathematics

University of Denver

_____

In Partial Fulfillment

of the Requirements for the Degree

Doctor of Philosophy

_____

by

Aml Abd Alhamed Alnaas

November 2016

Advisor: Michelle K. Knowles

Author: Aml Abd Alhamed Alnaas
Title: C-REACTIVE PROTEIN INTERACTIONS WITH CELLULAR MEMBRANES AND SUPPORTED LIPID BILAYERS
Advisor: Michelle K. Knowles
Degree Date: November 2016

ABSTRACT

C-reactive protein (CRP) is a serum protein that binds to damaged membranes and initiates the complement immune response. Different forms of CRP are thought to alter how the body responds to inflammation and the degradation of foreign material. Despite knowing that a modified form of CRP(mCRP) binds to downstream protein binding partners better than the native pentameric form, the role of CRP conformation on lipid binding is yet unknown. In this work, three main assays were performed to characterize how conformation affects CRP-membrane interactions. The first assay utilized supported lipid bilayers that mimic the plasma membrane of apoptotic cells. The results show that CRP interactions vary with protein conformation, lipid composition, and membrane shape and that the mechanism by which CRP recognizes damaged membranes depends on the combination of all three. The second assay focused on CRP interactions with cellular membranes by using induced apoptosis in MES-SA cells to characterize how CRP recognizes damaged cellular membrane. Monitoring the disassociation of pCRP to mCRP on apoptotic cell membrane with a fluorescent RNA aptamer that specifically binds mCRP but not pCRP allowed for quantitative analysis. Thirdly, a fluorescence quenching assay was utilized to characterize CRP conformational states using 8-anilino-1-naphthalenesulfonic acid (ANS), a fluorescence probe that binds to the hydrophobic regions of a protein. The unfolding of CRP using different denaturants was assessed using tryptophan fluorescence assay. Urea-EDTA, Guanidine-HCl, and

SDS with heat were used to perturb the pentameric state. All treatments give rise to a monomeric state in native PAGE experiments. As revealed by ANS fluorescence, treatment with 2.5M GndHCl, 3 or 6 M urea, or 0.01% SDS caused hydrophobic portions of CRP to be exposed. Based on this data, we conclude that the two forms of CRP studied here have different mechanisms of action.

ACKNOWLEDGEMENTS

In the name of Allah, most Gracious, most Merciful.

A word of thanksgiving to God, the source of all knowledge, by whose abundant grace this work has come to fruition.

A deep appreciation is expressed to Dr. Michelle Knowles for her great support and encouragement. A large depth of gratitude to my parents for their vital support. My thanks to my husband, brothers, sisters, and my son for their continual support. I would like to thank my friend Carrie Moon for her great support. My thanks are extended to the University of Denver and the faculty members of the chemistry and biochemistry department. I am grateful to the Libyan Ministry of Higher Education for funding support.

TABLE OF CONTENTS

LIST OF FIGURES

LIST OF ABBREVIATIONS

ANOVA - Analysis of variance

ANS - 1-Anilinonaphthalene-8-sulphonic acid

BAR - Bin-Amphiphysin-Rvs

CRP - C-reactive protein

CVD - Cardiovascular disease

DMSO - Dimethyl sulfoxide

EDTA – Ethylene di-amine tetra acetic acid

ELISA – Enzyme linked immunosorbent assay

FRAP – Fluorescence recovery after photobleaching

LDL – Low density lipoprotein

Lyso PC – Lyso phosphatidylcholine

MB-DPHE - Marine Blue 1,2- Dihexadecanoyl-sn-Glycero-3-phosphoethanolamine

mCRP – Monomeric CRP or modified CRP

NP – Nanoparticle

PAGE – Polyacrylamide gel electrophoresis

PC – Phosphocholine

POPC – Palmitoyl-oleoyl- phosphatidylcholine

pCRP – Pentameric CRP or native CRP

ROC – Radius of curvature

SDS –Sodium dodecyl sulfate

SLB – Supported lipid bilayer

SLIC –Single liposome curvature

TIRF – Total internal reflection fluorescence

CHAPTER ONE: INTRODUCTION

1.1 C- Reactive Protein (CRP)

Cardiovascular diseases (CVD) are one of the leading causes of death in the world. Annually about 16.7 million deaths are attributed to chronic inflammatory diseases of the arteries and atherosclerosis[1]. In the United States around 610,000 cases of myocardial infarction every year are attributed to atherosclerosis[1]. The mortality rates of CVD have been reduced by 33% in the last 20 years due to improvements in treatment and early prevention. However, the elevated rate of current incidence requires researchers to develop treatments that prevent CVD[1]. Clinically, C-reactive protein (CRP) is a good indicator and a risk factor for CVD[2], [3]. CRP has been shown to accumulate at sites of inflammation[2], [3] and an elevated level of CRP is linked to chronic inflammation and cardiovascular disease (CVD)[3]. CRP was discovered by Tillet and Francis over 80 years ago and initially named C-reactive substance due to its reactivity and ability to precipitate the C- polysaccharide of the pneumococcus cell wall[4]. The blood plasma level of CRP rises dramatically in response to infection, tissue injury, and inflammation. CRP is a plasma soluble protein and acts as a marker for the cardiovascular disease (CVD)[3]. CRP levels in serum increase significantly and rapidly to 1,000 fold during the first 24-48 hours in response to inflammation. In 2003, studies demonstrated that people with slightly elevated levels of CRP, in a range between 3 and 10 μg/mL, are at risk for developing CVD, leading to CRP being used as a biomarker for

CVD[5]. This view was later revised when CRP was considered a participant and mediator in the formation of lesions and atherosclerosis due to its inhibitory effect of nitric oxide production by endothelial cells. Quenching the releasing of NO leads to the stimulation of endothelial cell apoptosis and inhibition of angiogenesis[5]. Studying CRP, a mediator and participant in CVD, will lead to a better understanding of the mechanism of plaque formation in heart disease.

CRP is a pentameric protein belonging to the pentraxin family, and is composed of five identical subunits (protomers) associated noncovalentaly[6]. The crystal structure of CRP was solved in 1999 and is shown in Figure 1. The crystallographic data shows that each promoter has binding sites for two calcium ions and one binding site for phosphatidylcholine (PC) on the recognition face of CRP (face B). The major interaction between PC containing ligands and CRP bound calcium ions occurs via a phosphate oxygen group of PC. The opposite face (Face A) exhibits binding sites for C1q, Fc receptor (FcR)[7], integrins[8] and C4b- binding protein[9].

CRP exists in at least two different conformations with distinct bioactivities. Native pentameric CRP (pCRP) and modified CRP (mCRP) are the most well studied forms. Previous work by Potempa in 1983 suggests that human CRP has two distinct forms, one is a native CRP (110 kDa) bound to PC, and the other as free subunits (22.5 kDa), which expresses a new epitope leading to different reactivity. mCRP binds to downstream binding partners, such as factor H, C1q and C4bp[10]. Five novel molecular forms of CRP in human plasma which are different from pCRP and mCRP have also identified recently with one form significantly linked to obesity.

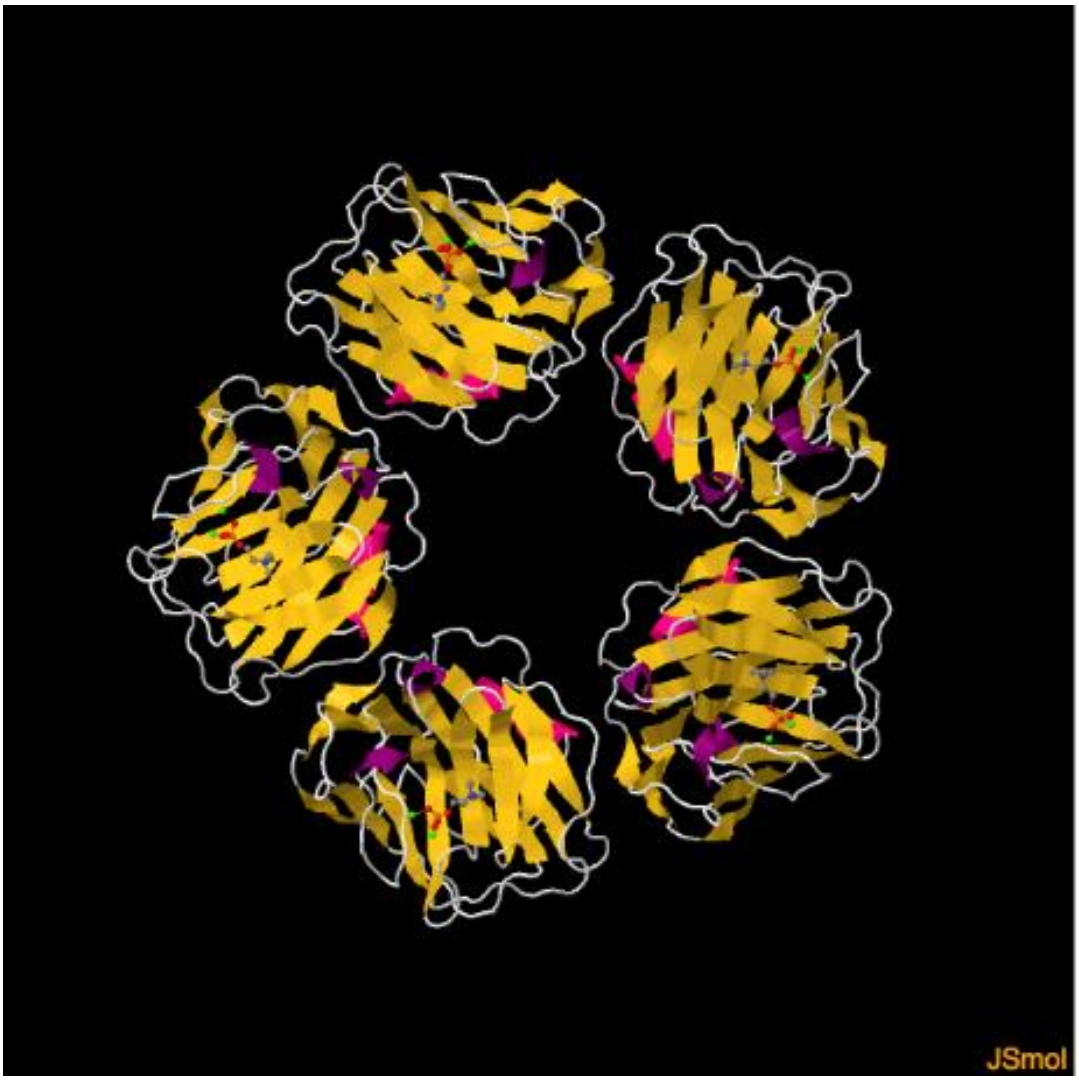

Figure 1. CRP crystal structure.
CRP is a pentameric protein binds one phosphocholine head group (grey/red structure in center of monomer) per monomer unit in a calcium dependent manner (Ca2+ is green, two per monomer). Image was taken from the protein data bank (PDB Identifier: 1B09), and the structure was solved by Devaraj, et.al.[11].

The main functions of CRP are to control inflammation, stimulate the clearance of tissue components and damaged cells, and to recruit damaged cells for phagocytosis[4]. In 1981, research showed for the first time that CRP has a protective activity against

Streptococcus pneumonia infection in mice[12]. CRP is involved in the activation of the classical complement pathway through its binding to different ligands which leads to the killing of microorganisms and the protection of the host. Among the ligands that mCRP is able to bind to activate the classical complement cascade, C1q binding is one of the most significant functions of CRP. mCRP binds C1q, which activates the complement response, and also C4bp[1] and factor H, both of which attenuate the immune response. The monomeric form of CRP leads to pro-inflammatory states by binding to integrin proteins on monocytic U937 cells[8].

By binding C1q as part of the classical complement pathway, CRP is involved with both the innate and adaptive immune system. CRP activates the classical complement cascade and promotes an anti-inflammatory response when it binds to an apoptotic cell surface, by increasing binding of C3b/bi and C1q[4]. CRP binding improves the phagocytosis of apoptotic cells by macrophages. CRP inhibits the alternative complement pathway by recruiting factor H to the cell surface which inhibits C5 convertase and prevents the formation of the membrane attack protein (MAC). Another important property of CRP is its binding to Fcγ receptors which leads to increasing phagocytosis and releasing of inflammatory cytokines[4].

Phosphatidylcholine (PC) is the most well described small molecule that CRP recognizes and binds to on the surface of damaged and apoptotic cells[2], [13]. The K_d for CRP-phosphorylcholine ineraction is 18μM[14]. It is not clear why CRP does not bind PC present on healthy cells. Past work has shown that lysophosphatidylcholine (lysoPC) and PC are recognized by CRP. Both of these lipid are common in damaged membranes, like apoptotic cells, but lysoPC is less common in healthy cells. It naturally occurs as a

result of partial hydrolysis of phosphocholine by the enzymatic action of phospholipase and represents ≤ 3.0% of the phospholipids in a cellular membrane[15]. It has also been shown that certain phospholipases or membrane damage cause PC to become more exposed and accessible to CRP [4]. Others have shown that the incorporation of lysoPC in the natural lipid bilayer induces positive curvature[16], by causing a disturbance due to acyl chain mismatch[17], and promotes CRP binding in phosphatidylcholine vesicles[18]. Also, lysoPC has been shown to mediate the binding and dissociation of pCRP on the surface of Jurkat T cells[19].

In addition to lysoPC, CRP shows binding activity to both oxidized LDL (OxLDL) and apoptotic cells by recognition of their phosphorylcholine moiety that becomes more exposed due to oxidation which leads to opsonizing them for macrophages.[13] Lipid oxidation leads to a conformational switch in the structure of phospholipids by making the fatty acid tail hydrophilic. This causes protrusion of oxidized fatty acids from hydrophobic moiety to an aqueous environment[20].

Beyond phosphatidylcholine oxidation, membrane curvature has been shown to enhance the binding of CRP to damaged membranes[21]. CRP shows curvature dependent binding to lipoprotein particle mimics (LPP) with high binding to LPP with diameter ≤ 28 nm. This binding causes CRP to disassociate to mCRP which expose a new epitope for C1q binding[21]. We hypothesize that both lipid composition and membrane curvature are factors by which CRP forms recognize damaged membranes for clearance.

The mechanism by which CRP converts to other forms has been discussed by others. pCRP dissociates on lipid monolayers that consists of egg PC/lyso PC into subunits as shown by Wang, et al in 2001[22]. As illustrated in Figure 2, pCRP loses its

pentameric structure and has a conformational rearrangement when it binds to an endothelial cell membrane, forming mCRP that deposits in the blood vessel walls[23]. Moreover, pCRP changes conformation and transforms to a modified form under acidic pH conditions that mimic the environment of the inflammation sites[24].

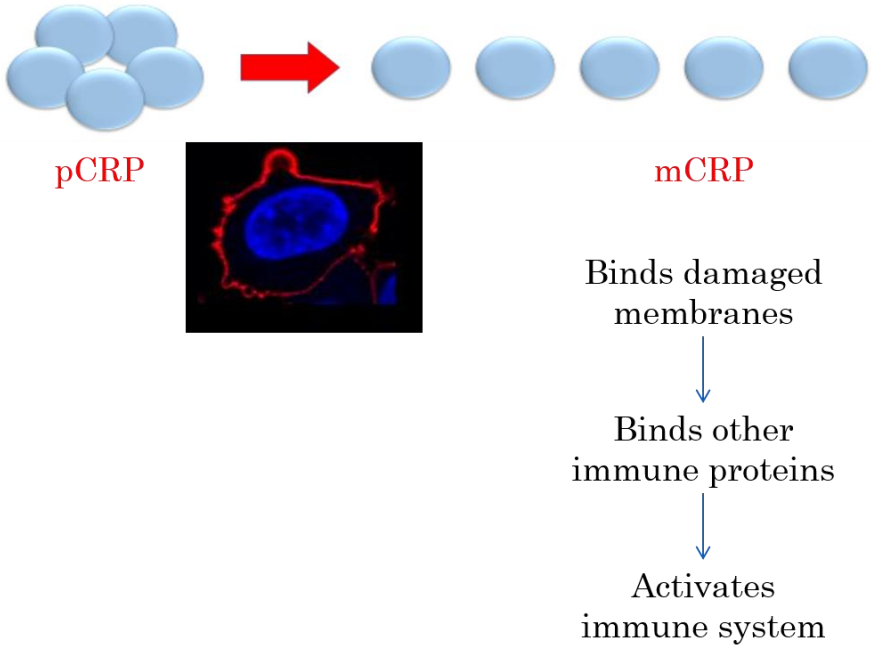

Figure 2. Conversion of pCRP.
Illustration of pCRP conformational changes upon its binding to a cell surface.

Beyond lipids, CRP also has well described protein binding abilities. CRP interacts with various complement proteins such as C4 binding protein and factor H which leads to the activation of the complement pathway through its binding to one molecule of C1q per two adjacent molecules of CRP bound to a ligand[9]. Research shows that mCRP which forms due to the disruption of the structure of pCRP using urea is able to bind factor H and C4BP. However, native pCRP did not bind. In addition to complement proteins, integrins have been identified to be binding partners for CRP[8].

Two novel receptors for mCRP were discovered and their binding linked to the pro-inflammatory action of mCRP binding to U937 cells. In contrast, pCRP showed less effective binding to these integrins, which was attributed to an increased steric hindrance due to size[8].

Cholesterol has also been identified as a novel ligand for CRP. The presence of cholesterol binding domains within CRP suggests that the non-esterified cholesterol content on the LDL surface has a role in CRP binding to modified LDL.[25] CRP has been shown to opsonize native LDL which may play a role in foam cell formation and atherogenesis[26].

1.2. C1q

C1q is an early component of the classical complement pathway and is known to bind CRP. It is a well-recognized protein of the innate immune system[27]. C1q is a 460 kDa protein formed from six hetero subunits with each unit containing collagen-like trimeric helical fibers. Each of these subunits ends with a C-terminal globular region which binds to the apoptotic cell surface. C1q participates in the maintenance of the immune tolerance via phagocytosis[28].

Previous studies have shown that C1q recognizes and binds to the phosphatidylserine (PS) exposed on the surface of apoptotic cells through its globular region at an early stage of apoptosis and allows for efficient apoptotic cell clearance. The dissociation constant for the interaction of C1q globular regions with PS is $7x10^{-8}$ M. C1q has showed to bind to blebs isolated from apoptotic cells and activates the complement

pathway. The C1q globular region forms a complex with phosphoserine through the interaction with subunit C of the globular region[28].

CRP binding to C1q has been showed to trigger the activation of the classical complement pathway. The binding site of C1q on CRP was defined by Agrawal in 2001. Research showed the Asp^{112} and Tyr^{175} residues are important for the C1q binding site located at the end of the open side of the cleft on the promoter on the pentameric face opposite to the PC binding site[29]. The dissociation constant for the interaction of C1q with pCRP was determined to be 1.45 nM[9].

1.3 Membrane Curvature

Lipids and proteins are involved in membrane deformation and curvature. Thus, changes in the lipid composition can cause membrane curvature and influences the morphology of the membrane[26]. Lysophosphatidylcholine (LysoPC) tends to form an inverted cone shape and generates positive curvature upon its addition to the lipid bilayer[12.] LysoPC is produced as a result of phospholipid hydrolysis by the phospholipase enzyme A2 in position 2 of phosphoglycerides[27.] Cellular membranes have different compositions of lipid that vary throughout the cell. LysoPC is a naturally occurring detergent that accounts for ≤ 3% of the lipid bilayer. The outer leaflet of a eukaryotic plasma membrane is mainly composed of phosphatidylcholine (PC) which makes up more than 50% of the phospholipids. In contrast, the cytosolic leaflet of the membrane is enriched with phosphatidylserine (PS) and phosphatidylethanolamine (PE) [26].

The presence of lysoPC has long been known to enhance CRP binding to damaged cell surfaces or on the surfaces of artificial bilayers. Previous work showed that

the incorporation of lysoPC to PC liposomes led to a change in the geometry of the lipid model and caused a mismatch in the lipid bilayer that makes PC head groups more exposed and accessible to CRP to bind[18]. Binding between CRP and lysoPC has an impact on atherosclerosis[30]. CRP complexed with lysoPC has been shown to restrain pro-atherogenic effects on macrophage cells which in turn may delay the atherosclerosis progression.

Phospholipids with two saturated acyl chains exhibit a cylindrical shape, inducing no curvature. Cone shaped lipids form if the head group is significantly smaller than the acyl chain area and lead to the generation of negative curvature (concave) with a smaller surface area. This forces the head groups to be close together against electrostatic repulsion and cause steric hindrance[12]. This configuration is energetically unfavorable in biological systems and can be stabilized by changes in lipid composition and the presence of certain proteins at curved regions, which facilitate protein binding to accommodate membrane deformation. Phospholipids that have a smaller acyl chain area than the head group form an inverted cone shape and generate an area of positive curvature (convex) with packing defects in the positive face[12]. The density of the hydrophobic defects would increase as a result of membrane bending, and the increasing in the surface area of the positive face will cause the hydrophobic tails to be exposed to the aqueous environment which is an entropically unfavorable situation. Increasing the density of the defects leads to the recruitment of large densities of hydrophobic molecules, [27] such as lysolipids that have single tails to fill the gaps and stabilize the hydrophobic defects. Figure 3 illustrates the structure of these lipids.

Some proteins, including BAR domains and amphipathic helices, are known to bind to curved membranes. Extreme membrane curvature within the cell can occur in different structures such as the golgi, endoplasmic reticulum, microvilli and the plasma membrane[26]. Plasma membrane curvatures play a vital role in cellular function.

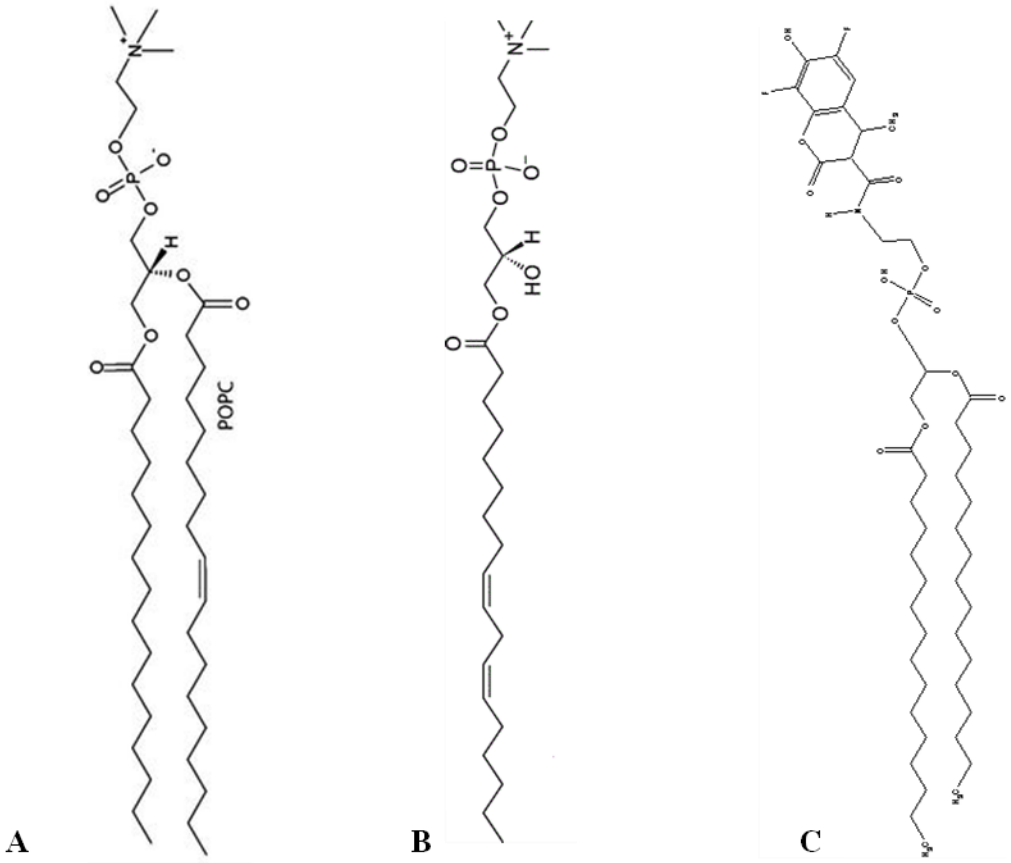

Figure 3. Chemical structure of lipids and dye labeled lipid used in this work. A) POPC [31], *B) lysoPC*[32] , *C) MB-DHPE*[33].

Beyond lipids, proteins are also involved in membrane deformation generating positive and negative curvatures. Amphipathic helices that have one polar charged face and one hydrophobic face promote membrane curvature via asymmetric insertion into one leaflet of the membrane, which causes a wedge in the membrane and generates

curvature. The hydrophobic face dips into the tail section of the bilayer while the polar face interacts with the polar head group of the membrane[34].

Another mechanism by which cells deform lipid membranes is through the use of proteins. Scaffolding by proteins that have a rigid structure is one of the mechanisms that influence membrane curvature. Common examples of these proteins are the dynamin family of proteins that bind to inositol lipids and constrain tubular shape in the membrane. BAR domain proteins and banana shaped dimer proteins are considered to be sensors for highly positive curvature. These proteins bind strongly to highly curved membranes due to an increase in the area of electrostatic interaction and a matching of the intrinsic curved area of the protein with the area of curved membrane. Another aspect of BAR proteins is their interesting interaction with the N-terminal of an amphipathic helix (N-BAR domains) which induce positive curvature upon their insertion into the lipid bilayer.

Due to the complexity of the biological cellular membrane, it is a challenge to study how the membrane curvature and lipid shape affect molecule binding. Moreover, it is difficult to separate the shape of the membrane from the chemical compositions within the cell. Therefore, different methods have been proposed to mimic cellular membranes. One of these established methods uses a single liposome curvature assay (SLiC) to study membrane curvature sensing of biomolecules[25]. In this assay, liposomes of different curvature were labeled using a fluorescent lipid and immobilized on a glass surface. The size of the liposomes was determined from the relative fluorescence. The protein of interest was labeled with a different fluorescent dye and the density of bound protein was calculated from the fluorescence intensity extracted from the images taken by confocal

microscopy. The advantages of using this assay is to exclude the ensemble averaging error which can arise when polydispersity exists. The major disadvantage is that the liposomes are isolated, so the bound molecule cannot undergo dynamic exchange along the surface as in the plasma membrane.

Another group used a wavy glass substrate with continuous positive and negative curvature[26]. The liposomes were deposited on the surface to form a supported lipid bilayer (SLB). The advantage of using this method is that it has a transition between the area of positive and negative curvature. One disadvantage is that this method requires two different processes to characterize the curvature and to visualize the bound protein which requires another method to correlate them. The main disadvantage is that the lacking of highly curved regions. Moreover, preparing the glass requires high temperature and using a prefabricated mold which makes changing the topology of the glass to be used in different experiments difficult.

To overcome these limitations, our lab has developed a cell membrane mimic biosensor which is done in a way that allows us to separately change the shape and chemical compositions[35]. This is one of the main advantages of the system since it is challenging to do that in the biological system. Also, the spatial resolution between the protein of interest and the sites of curvature can be achieved by using this biosensor. The sites of curvature in this model are separated, so the equilibrium dynamic between the flat region of the membrane and the sites of curvature was permitted which mimic the blebs surface in the cells. This will help us to understand how CRP recognizes apoptotic cells and oxLDL but not healthy cells and intact LDL. Also it will help us to know what causes

the CRP conversion to mCRP which in turn binds C1q and leads to the activation of the complement system. Moreover this assay will allow us to know if the membrane shape affects CRP function.

Briefly, the SLB was formed over fluorescent polystyrene nanoparticles 40 or 100 nm diameter that were deposited upon a flat glass surface. Liposomes were prepared by probe sonicating lipid films and lipid bilayers were created when liposomes fused with the surface[35]. Figure 4 shows the biosensor with the regions of positive, negative, and no curvatures. Fluorescent nanoparticles with different radii are used to control the extent of curvature.

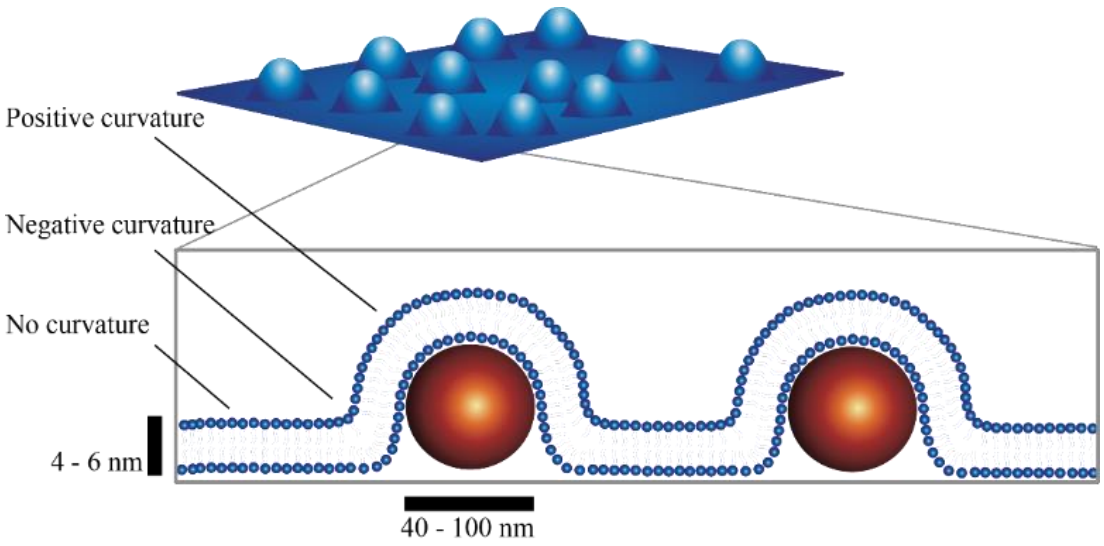

Figure 4. Cell membrane mimic biosensor model.
Lipid bilayer formed on the top of fluorescence nanoparticles showed regions of positive, negative, and no curvature. Note that the lipids and nanoparticles are not drawn on the same scale.

1.4 Overview

This dissertation is divided into five chapters. Chapter two describes Characterizing the membrane curvature assay and discuses in details the quantitative analysis methods and programs that we used to quantify the data. It also focuses on investigating how lipid compositions and CRP forms affects binding to curvature. Chapter three focuses on using cellular membrane to characterize CRP binding to apoptotic cells using MES-SA cells. Chapter four discusses using fluorescence assays to characterize CRP conformational change. Finally, chapter five summarizes the major results.

CHAPTER TWO

2.1 Conformational Changes in C-reactive Protein Affect Binding to Curved Membranes

This Chapter details the preparation of the curved supported lipid bilayer (SLB) to investigate whether or not CRP preferentially binds to curved membrane. The SLB enables us to separately quantify how the lipid composition and membrane shape affects CRP recognition membrane. In addition, the different conformations of CRP (pCRP and mCRP) affecting its binding to curved membranes was characterized. Fluorescence recovery after photobleaching technique (FRAP) was also used to test the fluidity of the lipid to ensure that the SLB mimics the biological system.

It has been shown that the conformational changes in CRP affect protein-protein interactions, but little attention has been given to how protein conformational changes affect lipid binding. It is interesting to note that PC is the predominant lipid headgroup in the outer leaflet of cell membranes, yet CRP does not bind PC present on the surface of healthy cells. Beyond Ca^{2+}, it is not clear what is needed for CRP to bind to lipid membranes. Past work has shown that lysoPC and oxidized PC are recognized by CRP. Both of these lipids are common in damaged membranes, like apoptotic cells, but less so in healthy cells. Others have shown using mimics of LDL that neither lysoPC nor oxPC are needed; instead, CRP can recognize PC when it is presented on very small (diameter <30 nm) nanoparticles[21]. In this work we show that the shape of the membrane can

recruit CRP; curved membranes bind more CRP. Modified CRP binds curvature, but the soluble pentameric CRP does not over the range of curvatures tested.

2.2 Materials and Methods

2.2.1 Supported Lipid Bilayer

Lipid films in this study were prepared by using 1-palmitoyl-2-oleoyl-sn-glycero-3-phosphocholine (POPC) (Avanti Polar Lipids, 850457C) as the main component. In addition lysoPC (Avanti Polar Lipids) and marina blue 1,2-Dihexadecanoyl-sn-Glycero-3-Phosphoethanolamine (MB-DHPE) were used. The molar ratio of these components are varied as desired.

Our lab has developed a supported lipid bilayer (SLB) membrane mimic as described previously[35].The SLB was formed over fluorescent, carboxylate-modified polystyrene nanoparticles (FluoSpheres, Life Technologies;40-100 nm diameter) or over a flat surface. The nanoparticles were first diluted to (1:1000) in deposition buffer and sonicated in a bath sonicator for 15 minutes. Then, the second dilution of the sonicated nanoparticles was made to a ratio of (30:700) before their deposition onto the 8 well plate (Lab-Tek® Chambered Borosilicate Coverglass System, Thermo Fisher). 100 µl of the diluted nanoparticles was added to each well and incubated for 30 minutes at room temperature. After deposition, the nanoparticle solution was removed from the plate prior adding the lipid. Lipid compositions consisted of PC, lysoPC, and MB-DHPE were dissolved in filtered chloroform and stored at 4 ^{0}C. PC (85% or 98%), lysoPC (14% or 3%), and MB-DHPE (1% or 2%) were combined as desired in batches with a total of 250 nmol and then dried under vacuum overnight to remove the chloroform. Upon use, a vial is filled with 2 mL of buffer (2 mM $CaCl_2$, 30mM HEPES, 140 mM NaCl or 2 mM

$CaCl_2$, 30mM PIPES, 140 mM NaCl pH 6.4) and was probe sonicated for 15 minutes. 100 μL of sonicated lipid solution was deposited in an 8 well plate and incubated at 37 °C for 1 hour. 50 μg/mL CRP or 50 μg/mL mCRP were incubated with the lipid bilayer at 37 °C for 2 hours. Primary anti-C-reactive protein (C6), mouse IgG monoclonal antibody (Santa Cruz Biotechnology) and secondary goat anti-mouse immunoglobulin G with Alexa 488 (Life Technologies). Primary and secondary antibodies were pre-incubated together in 1:1000 ratios for 30 minutes at room temperature. 100 μl of pre-incubated antibody solution was added to each well. Imaging was done on both total internal reflection fluorescence (TIRF) microscopy and laser scanning confocal microscopy.

2.2.2 Preparation of mCRP

Modified CRP (mCRP) was prepared by treating native pCRP with SDS diluted to 0.01% in HEPES buffer (30mM HEPES, 140mM NaCl, 2mM $CaCl_2$, or 30mM HEPES, 140mM NaCl, 2mM $CaCl_2$, pH 6.39) and heating it at 80^0C for an hour. pCRP was diluted to a final concentration 100 μg/mL. The conformational state of CRP was determined by using native polyacrylamide gel electrophoresis due to the different properties of pCRP and mCRP including running differently on a gel.

2.2.3 Image analysis of flat membranes

To analyze the binding of CRP to the membrane, Image J was used to identify spots in the protein channel that were saturated. Then, MATLAB was used to find the average intensity of the image without including the saturated pixels or the pixels that had an intensity of zero, which were the bright spot that were cut.

2.2.4 Location guided averaging analysis

Computational analysis of the images was done using location guided averaging analysis procedure in MATLAB statistical software. To find locations of curvature marked by red fluorescent nanoparticles, spots-finding methods were used based on freeware designed from the methods of Crocker and Grier[36]. The MATLAB code for these are found on the website by Blair and Dufrense[37]. Only the spot finding portion of the code was used for this work. Location were excluded if they were 9 pixels of another location or within 12 pixels of the image edge. Square regions of 25 by 25 pixels were cropped from images of the nanoparticles channel which represents the curvature location. The same region of corresponding locations in the protein channel were also cropped yielding pairs of images. All the cropped regions in each channel were averaged using ImageJ software to obtain a single image of 25 by 25 pixels of all the stacks. From the pairs of images, we measured the distribution of 1) Pearson's correlation coefficients and 2) intensity in the 5 pixels center minus a local background consisting of an annulus 1 pixel wide with a diameter of 13 pixels (ΔF). From the average of the green cropped images, a radial average was calculated. This is done by averaging all pixels that are a specific distance from the center pixel. For example, there are 4 pixels that reside one pixel (124 nm) away from the center (green squares) and these are averaged to give the second data point. Four pixels that reside 175 nm from the center are averaged to give the third data point and so on. MATLAB code for the radial averaging function is available upon request. The correlation function calculation was obtained Dr. Justin Taraska[38].

dF and radial plot measurements have been used by others to quantify the amount of the protein at region of interest[38], [39].

The Pearson correlation coefficient (PCC) is a well-established method to quantify the colocalization degree between two fluorophores from a pair of images. It has been used to map protein association with exocytic vesicles and endocytic structures[38], [39]. PCC has range from +1 to -1, where +1 denotes strong positive correlation, -1 strong negative correlation, and 0 indicates the absence of relation.

To calculate PCC, small regions (25x25 pixels) are extracted from the nanoparticle image (red) along with the corresponding regions from the proteins image (green). As a control, random positions are selected, cropped, and processed in the same way. Then, all images are first normalized by subtracting the average. A deviation from the average is a fluctuation. If the fluctuations in one color match the fluctuations in another color then that is a correlation. After subtraction, the green image was multiplied by the red (each pixel is individually multiplied) then the average of all 25 x 25 pixels was divided by the average intensity of individual images as shown in the following equation:

$$r = \frac{\sum(R_i - R_{av})\cdot(G_i - G_{av})}{\sqrt{\sum(R_i - R_{av})^2 \cdot \sum(G_i - G_{av})^2}} \qquad \textit{Equation 1}$$

When comparing different sized curvatures the surface area difference of the lipid bilayer was corrected as follows: the structure of the curvature was estimated to contain two parts: 1) a cylinder with a height equal to the radius of curvature (ROC) and a diameter of 2 times the ROC and 2) a hemisphere with a radius equal to the ROC sitting

on top. The amount of surface area normally present in a flat bilayer is equal to a circle with a radius equal to the ROC. The difference between the two is the increase in surface area due to the presence of curvature. For an ROC of 25 nm, the increase in surface area is 2-fold. For an ROC of 55 nm, the increase in surface area is 4.84-fold. This correction is performed in *Figure 22*, where different curvatures are directly compared.

2.2.5 Confocal microscopy

Laser scanning confocal microscopy is a powerful tool that illuminates a small region of specimen by utilizing a small pinhole aperture that allows just for the light comes from the area of interest to pass throw it and rejects the out of focus light. In this work, the Olympus FV 1000 laser scanning confocal microscopy was performed and a 100x oil objective (2x zoom) such that one pixel was equal to 124 nm and with numerical aperture (NA= 1.4). Three channels, blue, red, and green were used to sequentially excite the DHPE-Marine Blue with 405 nm with an emission window from 42 5nm to 475 nm, red nanoparticles were excited with 594 nm with an emission window from 575nm to 675 nm, and CRP with 488 nm diode laser with an emission window from 500 nm to 545 nm, respectively. The speed of the scan was 12.5us/pixel.

2.2.6 TIRF Microscopy

Total internal reflection fluorescence microscopy (TIRF) is a method primarily used to illuminate the fluorophores that are very close to the adherent cell surface or coverslip sample within 100 nm with an exponentially decreases in the excitation field[40]. The advantages of using TIRF are to reduce the background fluorescence due

to reducing the intensity of the fluorophores that away from the coverslip. Moreover, highlighting the events close to coverslip-sample interface. To achieve TIRF, the angle of incident Θ must be larger than the critical angle Θ_c as well as the refractive index of the glass n_2 should be greater than the refractive index of the sample n_1.

2.2.7 Fluorescence recovery after photo bleaching (FRAP)

Fluorescence recovery after photo bleaching is an optical technique intended to use for Characterizing lateral diffusion of lipids within a cellular membranes[41]. To mimic biological membrane, the supported lipid bilayers formed in our lab should be fluid. To examine that, a circular region of 125 pixels by 125 pixels (ROI) was bleached using laser beam at 100% with 405 nm wavelength by laser scanning confocal microscopy. The emission was detected from 425nm to 475nm. Three initial frames were imaged before the photo bleaching, seven frames were taken after bleaching the bleached, and the total of 40 frames were imaged to obtain the recovery. The frames were taken at 1 frame per 0.5 s. The speed of the scan for imaged frames was 2 µs per pixel. To analyze FRAP images, Image J and GraphPad Prism were used.

The average intensity of the photo bleached area (ROI) for all images was corrected to the intensity of a region apart from ROI (reference area). The mean intensity of ROI measured in each experiment was normalized. The intensity of the first image was set to 1 since it has a highest value in image series. The lowest value was set to 0 which represent the intensity of the frame immediately followed the step of bleaching.

2.3 Results and Discussion

The main goal of our work is to detect what recruits CRP to bind the lipid membrane and determine how the conformation of CRP affects binding. To do so, two factors were addressed, the lipid bilayer composition and the degree of the membrane curvature. The membrane curvature assay used in these experiments allows for control the composition of the bilayer independently from the bilayer curvature. First, we examined the effect of introducing lysoPC to the membrane containing POPC, which is a CRP binding site as shown in figures 4 and 5. Second, we tested the effect of membrane curvature on recruiting CRP.

In order to mimic the biological system, it is very important for the SLB to be fluid. Therefore, the lipid fluidity was tested using FRAP technique before all the experiments were performed.

2.3.1 Fluid lipid on a patterned substrate

FRAP experiments were performed to measure the MB-DHPE percent recovery, diffusion constants, and mobile fraction on a flat surface or curved membrane (40nm, 100nm nanoparticles). ImageJ was used to retrieve FRAP data as described previously in section 2.2.6. Briefly, a region with diameter (125x125 pixels) was bleached using 100% laser power. Then lipid recovery was obtained by measuring a total of 40 frames.

After correcting for photobleaching as described above in method section, the following equation was used to fit the data to a curve.

$$F_t = F_0 + (F_\infty - F_0) * (1 - e^{-kt}) \qquad \textit{Equation 2}$$

$F_{t,}$ 0, ∞ represents values of fluorescence at given time, initially, and equilibrium, respectively. Then the following equation was used to directly calculate the half time

$$\tau_{½} = \frac{ln(2)}{k} \qquad \textit{Equation 3}$$

The diffusion constant, *D*, is related to the square of radius, *r*, of the bleached area, the half time, $\tau_{½}$, and a constant of the bleach shape, γ_D, as:

$$D = ({r^2}/{4\tau_{½}})\gamma_D \qquad \textit{Equation 4}$$

A representative FRAP series of MB-DHPE is illustrated in

Figure 5. Frames were taken at 1 frame /1.25 s.

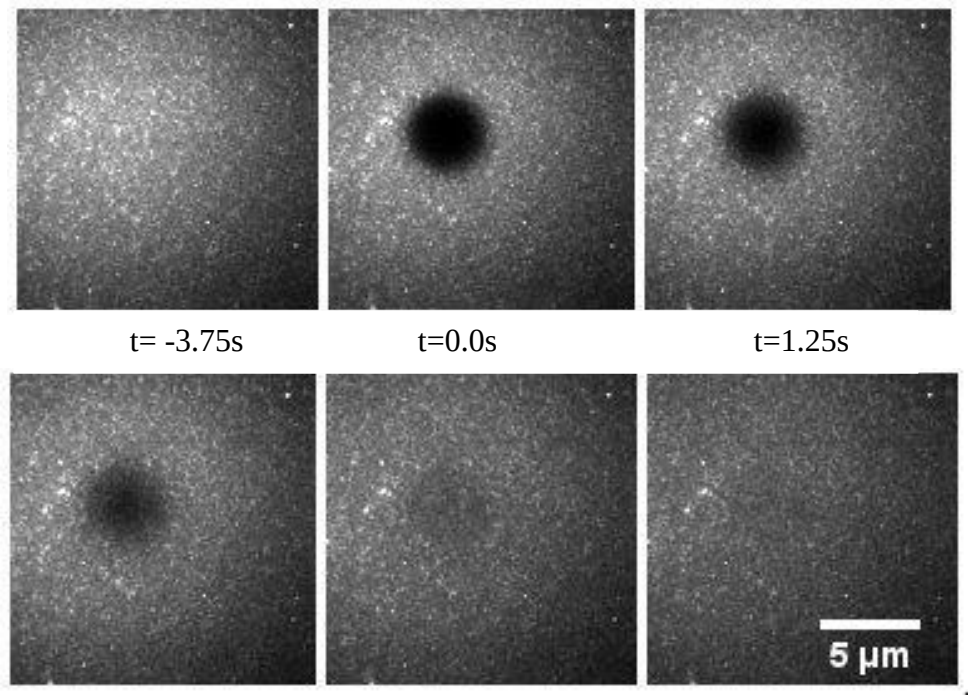

Figure 5. Fluidity of lipids measured by FRAP technique.
Series of MB-DHPE lipid FRAP images show intensity recovered in the bleached circle region in time. The bleach frame is at t=0.00s. The frame rate is 0.8 frame/sec. Images were corrected for overall photobleaching and the data was used to calculate lipid fluidity parameters (Figure 6).

FRAP was also used to test the fluidity of MB-DHPE on variety of curvature size using nanoparticles varied in diameter (45 nm, 100 nm), and a flat surface. The fluidity of MB-DHPE on POPC bilayers, POPC containing 3% of lyso PC bilayers, and on flat surface of POPC were tested. The recovery, diffusion constant, and mobile fraction are shown in figures 6, 7. Mobile fraction was obtained by dividing the average normalized intensities of the final three frames by the average intensities of the first three frames before photobleaching.

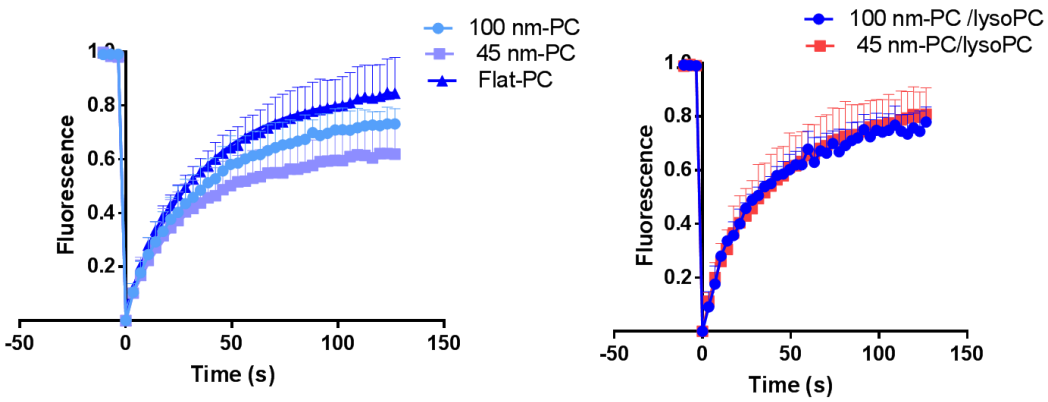

Figure 6. Lipid fluidity is measured by FRAP technique.
A) Average recovery of normalized intensity of lipid bilayers contains 98% POPC, 2% MB-DHPE are shown for 100 nm, 45 nm, and flat. The data shows the fit of 5, 3, and 3 experiments collected for 100 nm PC, 45 nm PC, and flat PC membranes respectively. B) Average recovery of normalized intensity of lipid contains 95%POPC, 3%lysoPC, 2% MB-DHPE are shown for100nm, 45nm. The data shows the fit of 4, and 4 experiments collected for 100nm PC/lysoPC, and 45nm PC/lysoPC membranes respectively.

FRAP data of the various recoveries of different lipid mixtures on either flat or curved surfaces is shown in Figure 6. Unpaired t-test revealed no significant differences between the recoveries over a curved surface with 100 nm and a flat surface ($p = 0.1656$) figure 6 A and between the two curved surfaces (100 nm, 45 nm) ($p=0.1491$). The recoveries of lipid bilayers containing 98% of POPC over a flat surface was significantly higher as compared with curved membranes with 40 nm diameter ($p = 0.0054$) figure 6 A. The recoveries of lipid bilayers contain 95% of POPC, 3% lysoPC over curved membranes (100 nm, 45 nm) showed no significant differences ($p= 0.842$) using unpaired t-test.

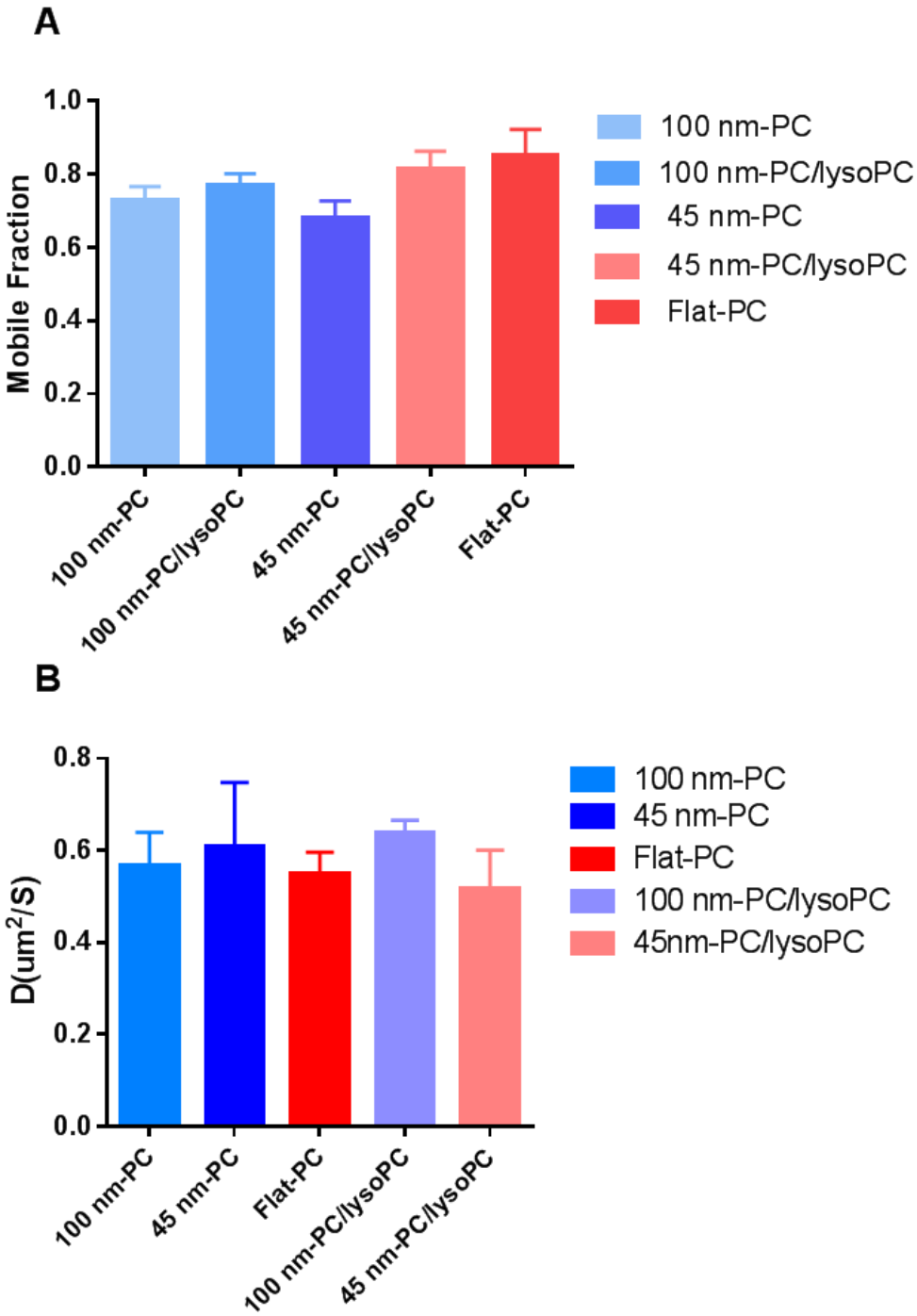

Figure 7. Lipid diffusion and mobility.
A) Comparing lipid fraction are not significantly different between the groups ($p>0.05$ ANOVA). Error bars represents SEM. B) Diffusion coefficient are not significantly different between the groups ($p>0.05$ ANOVA).Data represents the average of 5, 3,3,4,and 4 experiments collected for 100 nm PC, 45 nm PC, flat PC, 100 nm PC/lysoPC, and 40nm PC/lysoPC membranes respectively.

The fluidity of different surfaces was not significantly affected by changing the lipid composition and size of curvature. No significant statistical difference in diffusion constant, and in mobile fraction were obtained between the groups (P-value > 0.05 ANOVA) (Figure 7). Comparison of mobile fraction and diffusion constant between flat membrane and curved membrane is illustrated in Table 1.

Table 1. Comparison of Diffusion constant and mobile fraction between different lipid bilayer

Membrane lipid	Diffusion constant ($\mu m^2/s$) Mean/SEM	Mobile fraction Mean/SEM
POPC bilayer w/ 100 nm NPs	0.566 ± 0.073	0.729 ± 0.037
POPC bilayer w/ 45 nm NPs	0.594 ± 0.230	0.681 ± 0.046
POPC w/lysoPC bilayer w/100 nm NPs	0.638 ± 0.027	0.768 ± 0.032
POPC w/lysoPC bilayer w/45 nm NPs	0.516 ± 0.084	0.812 ±0.05
POPC bilayer w/o NPs	0.549 ± 0.046	0.849 ± 0.07

2.3.2 Influence of lipid type on CRP binding to a flat membrane

To test the effect of lipid type on CRP binding, pCRP or mCRP were incubated for 2 hours at 37^{o}C with flat lipid bilayer that contains 98%POPC and 2% MB-DHPE.

BSA was used as a negative control. Briefly, mCRP was prepared in our lab as described previously[42] by incubation of pCRP with final concentration of 0.01% SDS at 80 ^{o}C for one hour. The final concentration of pCRP was 50 µg/ml. mCRP runs as a monomer on a native polyacrylamide (supplement figure 1).

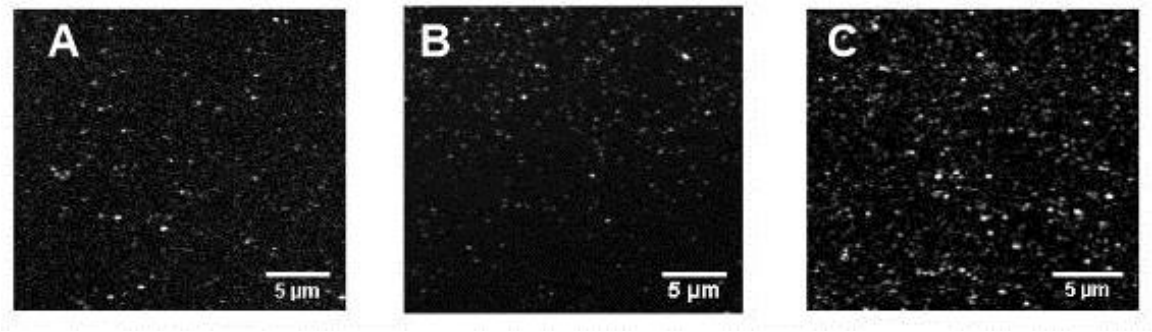

Figure 8. Influence of lipid type on CRP binding.
Fluorescent images of BSA (A), pCRP (B), and mCRP (C) binding to supported lipid bilayers contains 98% POPC and 2% MB-DHPE. CRP is labeled with primary D7 mouse antibody and secondary (Alexa-488 labeled anti-mouse monoclonal) antibodies.

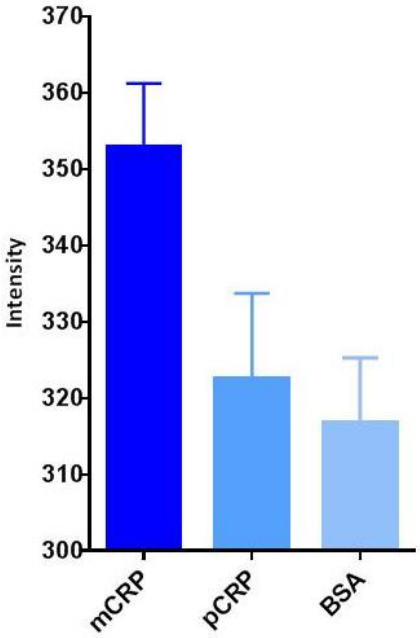

Figure 9. Average intensity of CRP binds to flat membrane.
Average intensity of BSA, pCRP, or mCRP binding to flat bilayers contains 98% POPC and 2% MB-DHPE. N=24, 29, 19 images for mCRP, pCRP, and BSA respectively, 3 experimental days. Back ground intensity was not subtracted. Error bar is SEM. Statistical significance was observed ($p<0.05$) between pCRP, mCRP, and between pCRP, BSA.

Confocal images showed that the flat SLB membrane with POPC recruited pCRP slightly less as compared with mCRP Figure 8B, C. Quantification of the image intensity using MATLAB revealed that there is no significant difference for pCRP and BSA binding to the flat membrane, while mCRP binds significantly more than pCRP and BSA with $p<0.05$ (Figure 9)

.

2.3.3 Incorporating lysoPC into flat lipid bilayer enhances pCRP binding

Since previous studies have indicated that the PC liposomes that contain lysoPC enhanced CRP binding[43], we sought to test the effect of introducing lysoPC to the lipid bilayer on the recruitment of CRP. The influence of introducing lysoPC at 14% to the lipid bilayer containing 85% of POPC and 1% of MB-DHPE on CRP binding is shown in Figure 10. Images acquired by using TIRF revealed an increase in CRP binding to the flat membrane with lysoPC.

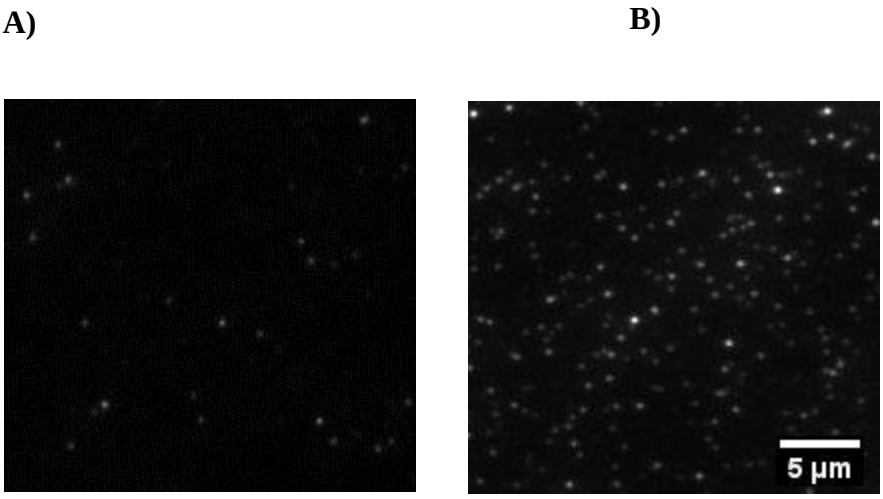

Figure 10. The effect of addition of lysoPC to POPC flat membrane on pCRP binding. A) TIRF images showing CRP binding to A) flat membrane contains 98% of POPC and B) flat membrane contains 84% POPC/ 14%lysoPC. Images are auto scaled.

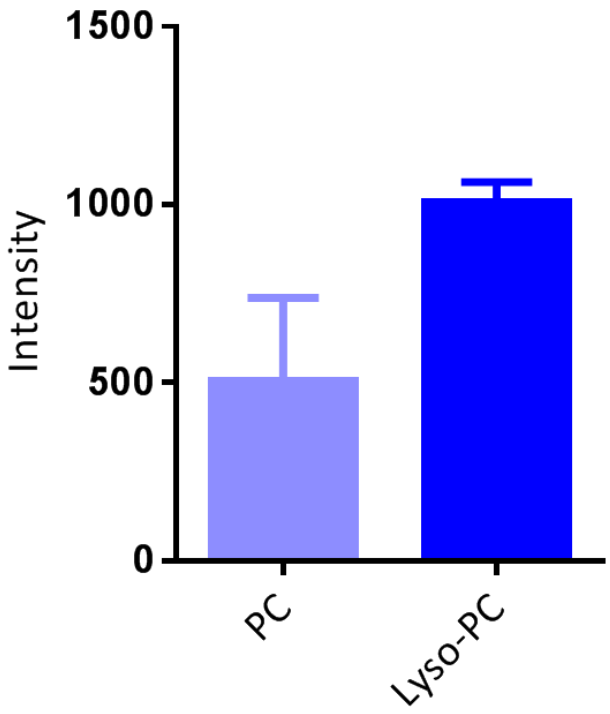

Figure 11. Average intensity of CRP binding to a flat membrane contains lysoPC. Average intensity of CRP binding to POPC or POPC-lysoPC flat membrane with the intensity of the antibody subtracted. N=12 images, 2 experimental days. CRP monoclonal mouse antibody C6 was used. No significant statistical difference was detected (p=0.299). The error is the SEM. Computational analysis was also performed to quantify the effect of lysoPC on CRP binding

Figure 11. MATLAB was used to find the spots for both images and detect their intensity. The intensity of saturated pixels which represents the cluster of the antibody molecules was not included in the total average intensity of each image.

TIRF images and the statistical data reveal that the membrane containing lysoPC recruits 50% more of CRP than the membrane that contains only POPC on flat membranes. The average intensity of the background was subtracted from the average intensity of CRP binding to both lipid membranes. Future work should be done to give a better understanding of the statistical difference between PC and lysoPC.

This finding is in agreement with previous work that showed incorporation of lysoPC to PC vesicles promoted CRP binding[18]. This is also relevant to a previous observation that showed association of CRP in *vivo* with membrane of altered or necrotic cells but not with the healthy cells[44] . This can be interpreted due to the restriction accessibility of polar PC head group to the water phase in intact membrane of healthy cells and not been freely accessible to CRP to bind. This is supported by NMR data that revealed the presence of intramolecular interaction between PC polar head group in artificial PC bilayers[45]. Therefore, it was suggested by Volanakis that binding of CRP to the PC polar head group in intact membrane requires disturbance in the bilayer geometry. This was tested by incorporating of lysoPC to PC bilayer which enhance CRP binding due to the relaxation effect that lysoPC cause to the restriction of accessibility of PC head group[18]. LysoPC is a single tail lipid tends to form an inverted cone shape and creates positive curvature.

Beyond assessing the effect of the flat membrane on CRP binding, we sought to determine whether curved membranes enhance CRP interactions with lipids using our membrane curvature assay described in Chapter 1.The following section illustrates in details the techniques that used to analyze the data.

2.3.4 Quantitative analysis of curved supported lipid bilayers

To determine whether or not CRP preferentially bound to curved membranes, supported lipid bilayers were created over a nano-patterned surface as described in methods section. Briefly, fluorescent nanoparticles were deposited at a density of 0.01-0.05 nanoparticles/$\mu m^{2.}$ CRP was incubated with the curved membrane surface and

labeled with green fluorescent antibodies. Two color, confocal imaging was performed to determine whether or not CRP bound to curved membranes. The red fluorescent nanoparticles mark locations of membrane curvature (Figure 12A), as demonstrated in previous work[35].The green fluorescent channel relates the amount and location of CRP (Figure 12B). The lipid bilayer is composed of MB-DHPE (2%) and POPC (98%), a common lipid on the cell surface, with regions of curvature that have a radius of curvature (R_{OC}) of 55 nm.

To quantify imaging data, nanoparticles were identified using a spot finding algorithm as described in method section. Nanoparticles that were separated by more than 9 pixels from other nanoparticles and more than 12 pixels from the edge of the images were cropped to 3.1 μm x 3.1 μm (25 x 25 pixel) images. The same locations were cropped from the CRP channel and three examples of single cropped images are shown in Figure 12C. The average of the nanoparticle images shows a spot in the center, as expected. The average of the CRP images also contains a spot, but when random locations are selected or BSA is used instead of CRP, no spot is detected (Figure 12C). This object-based method of data analysis yields pairs of images that can be further analyzed to obtain distribution information or averaged to obtain bulk information.

Because nanoparticles are very bright relative to the background and monodisperse in both size and intensity, it is straightforward to automate the identification of curved membrane locations. This is less true of CRP images. The variability in protein number yields a wider range of intensities and a more subjective measurement if spots were counted from this channel first. The identification of regions of curvature first allows us to automate our analysis using object-based or location-

guided colocalization methods[35], [38], [39]. From individual pairs of images the Pearson correlation function was calculated to relate how similar the two images are, with -1 being images that are opposites and +1 being identical. The distribution of correlation values is plotted as a histogram Figure 12 D and very little is observed to be correlated in samples containing pCRP and curved POPC bilayers, Figure 12 D, black bars. Random positions have a similar distribution, magenta curve.

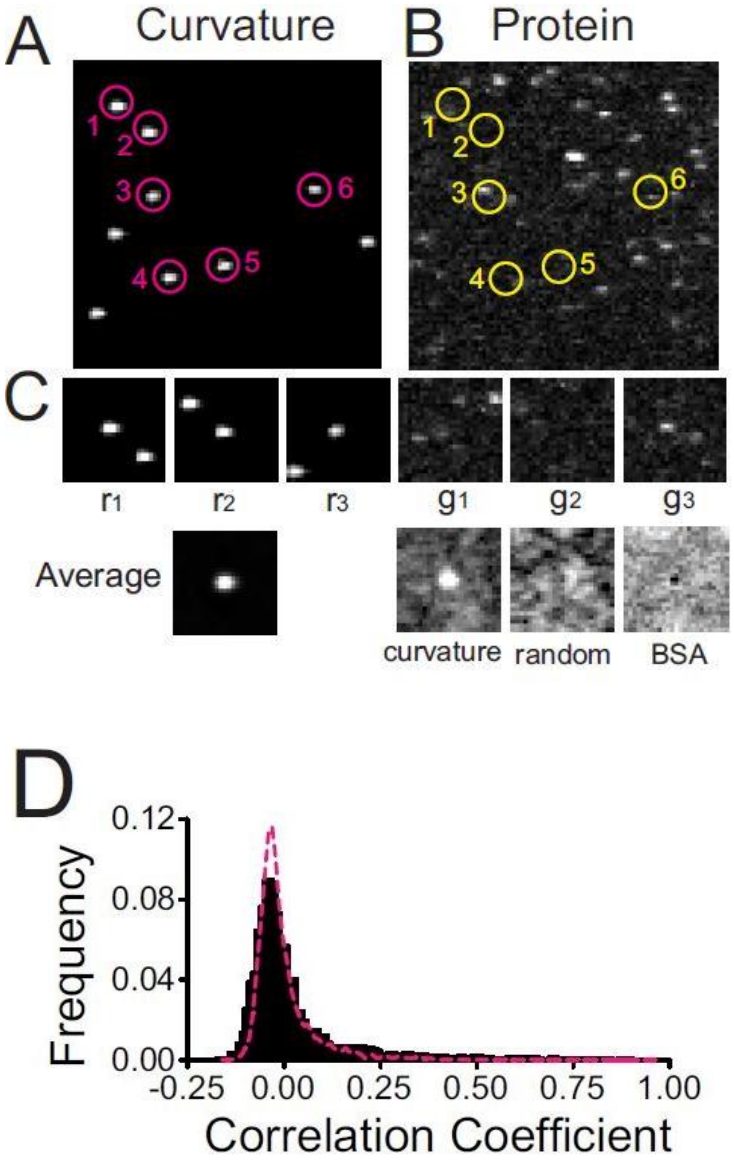

Figure 12. Description of the quantitative analysis of curved supported lipid bilayers. Supported lipid bilayers were created on a surface containing red fluorescent nanoparticles then imaged after incubation with CRP. A) Red fluorescent nanoparticles images mark sites of curvature. B) Green fluorescently labeled protein (pCRP) is imaged separately. Red positions are located using spot finding algorithms and positions are shown with circles. C) The positions that are > 13 pixels from the image edge and >9 pixels from another position are cropped to a 25 x 25 pixel region, where one pixel = 124 nm. The cropped locations are labeled with magenta circles 1-6. The same locations are cropped from the green image, shown in yellow circles 1-6, yielding pairs of images. Random positions are selected and cropped as a control D) The Pearson's correlation coefficient is calculated for image pairs and a histogram of all pairs of images is plotted for pCRP at regions of curvature (black) and pCRP at random positions (magenta dashed line).

The correlation function is useful for colocalization measurements, but the intensity information is lost so we performed another measurements that retain information related to the amount of protein present at curvature. All cropped, green (CRP) images (n=3297) were averaged and a radial plot of the intensity as a function of the distance from the center pixel was measured as shown in *Figure 13*.

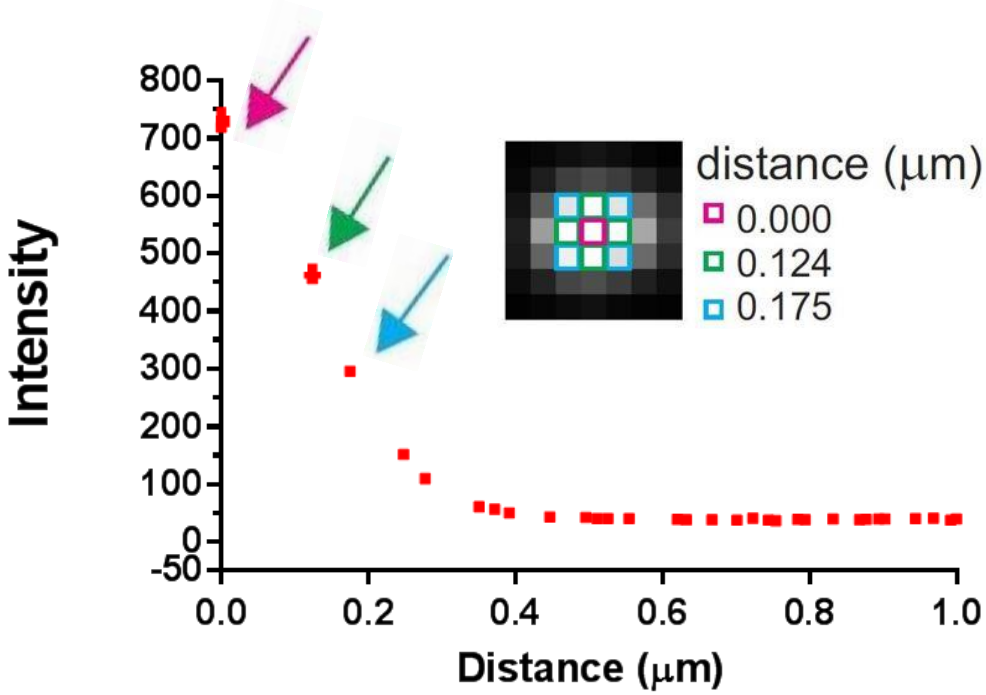

Figure 13. Radial plot calculation.
A radial plot of the average images is calculated in MATLAB by averaging all pixels that are a certain distance from the center pixel (shown in magenta). There are 4 pixels that reside one pixel (124 nm) away from the center (green box), and these are averaged to give the second data point (green arrow). Four pixels that reside 175 nm from the center (blue box) are averaged to give the data point shown beside the blue arrow and so on. The height of this plot at 0 nm is related to the amount of protein bound to nanoparticle positions. The offset at distances far from the center is related to the amount of protein that binds flat membranes, more than 1 μm away from curvature. The difference between the height and the offset, is related to how well the protein senses curvature relative to flat membranes. Background intensity was subtracted using the average intensity of the tail from the CRP monoclonal C6 antibody radial plot. The error is the SEM and it is smaller than the data points.

This is done by averaging all pixels that are the same distance from the center, as described in the figure caption and methods. After subtracting the background intensity, the intensity of samples lacking green fluorophores, there are two pieces of information in this plot: the height and the offset. The height is a measure of the amount of fluorescence at regions of curvature and the offset is a measure of the fluorescence due to binding to flat membranes. This method of analysis and these three measurements are used to quantify how the lipid composition, protein conformation and membrane shape separately affect CRP recognition of membranes.

2.3.5 CRP conformation affects binding to curved membrane

It is well known that the conformation of CRP affects binding to downstream proteins, such as C1q and Factor H [3]. Here we tested whether CRP conformation affects lipid binding to both curved and flat regions of membrane. Supported lipid bilayers containing 98% POPC and 2% MB-DHPE were created over top of a fluorescent nanoparticle patterned surface (ROC = 55 nm) then incubated with CRP and CRP antibodies. The modified form of CRP (mCRP) was made as previously described. In this preparation, the tertiary structure remains intact as demonstrated by the ability of mCRP to bind downstream partners of the complement immune response in a way that acid treated or fully denatured CRP does not[42]. Visually, mCRP shows high colocalization to nanoparticles sites and is also present in flat regions when compared to pCRP Figure 14A. The average of the cropped, nanoparticle images shows a spot in the center, as expected. All images, except the red fluorescent nanoparticle image, are scaled

identically and linearly for direct comparison. A spot appears in the center for mCRP, pCRP, samples with no CRP (and only antibodies, termed “none”), but not for samples where the surface has been blocked with BSA instead of CRP or when random regions are chosen instead of nanoparticle regions.

To assess the interaction between CRP conformers and curved membranes further, correlation coefficients were calculated from pairs of cropped images Figure 14B. mCRP (black bars) and pCRP (grey line) are different; mCRP has a higher correlation to the nanoparticle positions, suggesting higher preference for curvature. The average correlation coefficient is 0.29 for mCRP (Figure 14) and this is due to a large diverse distribution (Figure 14B). pCRP has an average of 0.03, which is similar to samples where no CRP has been deposited and antibodies alone accumulate at curved membranes. Randomly chosen positions show near 0 correlation. The data are illustrated in table 2.

positions	C_{avg}	STDEV	SEM	n
Curvature	0.29	0.26	0.004	3792
Curvature	0.03	0.14	0.002	3297
Curvature	0.04	0.16	0.004	1413
Random	0.0005	0.08	0.0024	1100

Table.2. Correlation coefficient values of CRP at sites of curvature

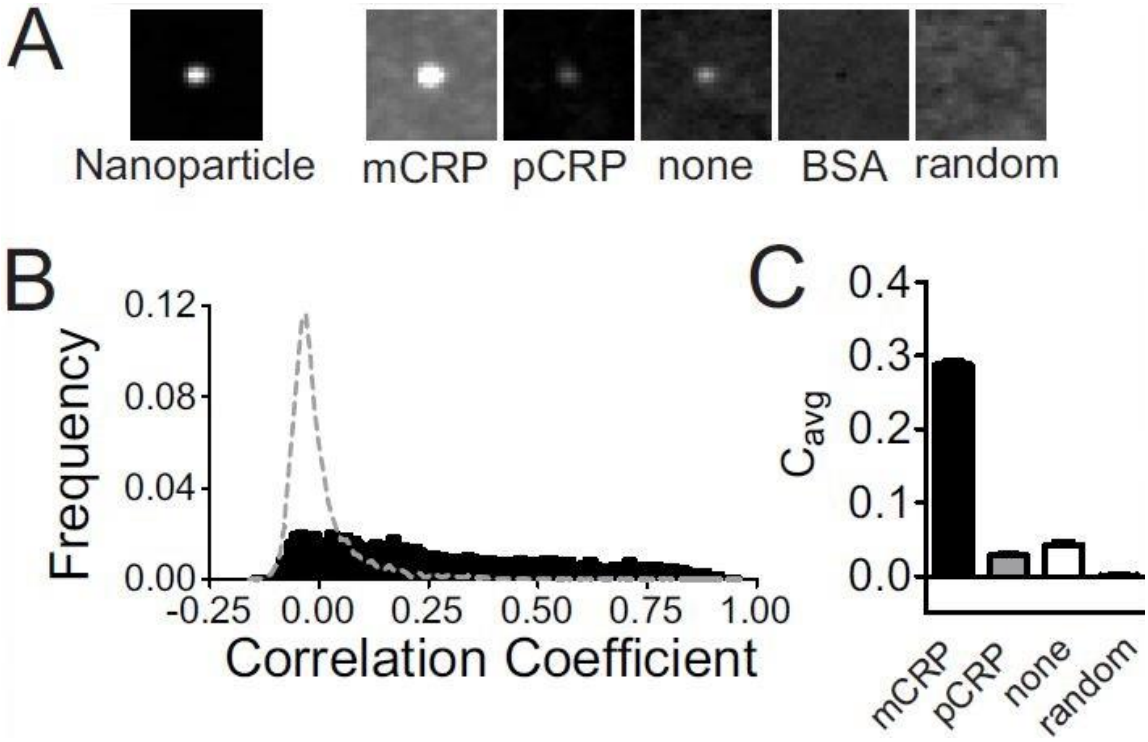

Figure 14. Protein conformational effects
Modified CRP and native, pCRP conformations of CRP are prepared and incubated on curved supported lipid bilayers, then imaged using confocal microscopy. A) Average images of nanoparticles, mCRP, pCRP, samples with antibodies only ("none"), and BSA blocked samples with antibodies only have been cropped from regions selected from nanoparticle positions. Random positions were also selected and mCRP regions were cropped from random positions (labeled "random"). The images are all scaled linearly and identically. B) The distribution of correlation coefficients for pairs of cropped images is measured for mCRP (black) and pCRP (dashed line). C) The average of the distribution is plotted for mCRP, pCRP, images with antibodies alone (no CRP), and CRP at random regions instead of curved membrane regions.

Modified CRP accumulates at curvature and the amount and distribution is quantified by plotting the radial distribution from an average image (Figure 15). The radial average of the cropped images shows that mCRP binds both flat regions, as

observed by the offset, and nanoparticle regions, observed by the peak height, better than pCRP.

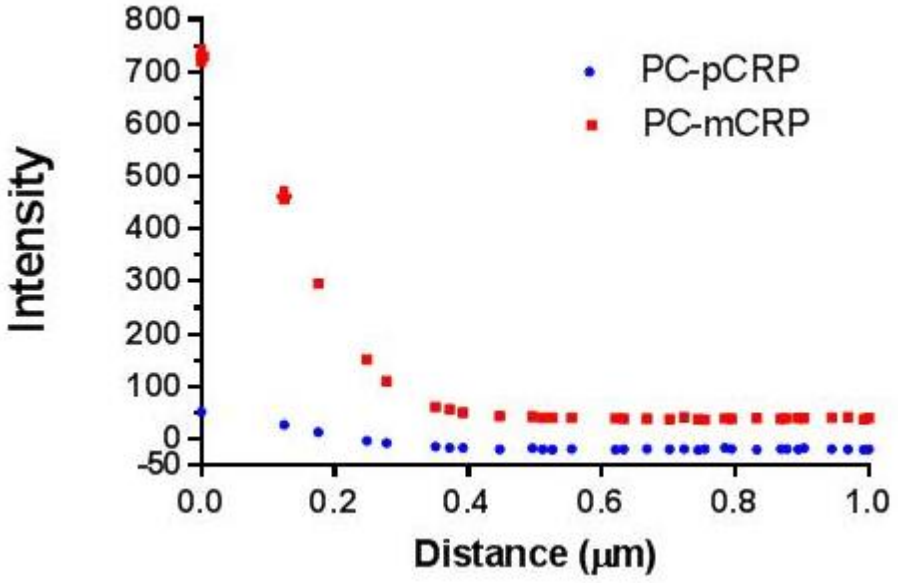

Figure 15. Comparing the Radial average intensity of CRP conformers at ROC (55nm). From the average images, the intensity is averaged radially to show the accumulation of mCRP and pCRP in both flat (large distance and curved (small distance) regions. Background intensity was subtracted using the average intensity of the tail from the CRP monoclonal C6 antibody radial plot. The error is the SEM

The increase in fluorescence at curvature relative to background, ΔF, is calculated from the height – offset for each cropped image, where the height is a pixel-weighted average of the first two points in the radial curve. The offset is measured 6 pixels away from the center, a distance greater than the spread of the intensity in the center but less than the nearest neighbor distance. In Figure 16, the average of all cropped images is plotted and ΔF is significantly higher for mCRP relative to pCRP.

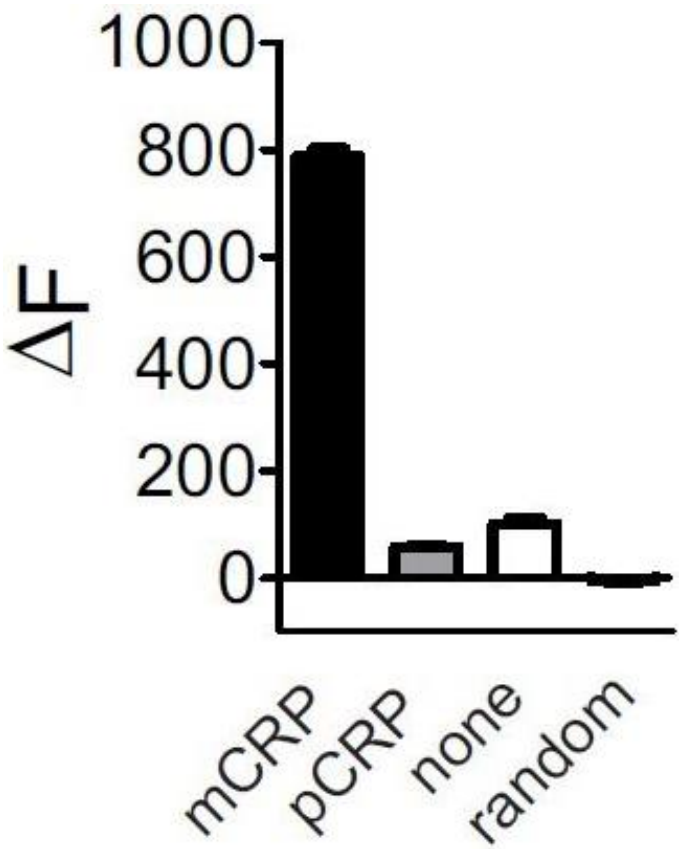

Figure 16. Average intensity of CRP conformers at sites of curvature.
The preference for curvature over flat regions, ΔF, is calculated from radial plots and the average of the distribution is shown. In all bar graphs, the error is the SEM.

The mCRP form was able to bind membranes significantly more than the pCRP form. This is likely due to hydrophobic regions of CRP being exposed once the pentamer is broken apart. Hydrophobic proteins preferentially insert into membranes or aggregate. In our work, we observe membrane incorporation and this membrane incorporation does not require Ca^{+2}. It is likely that any protein with hydrophobic parts exposed would show binding to curvature. Intrinsically disordered proteins were recently discovered to induce membrane curvature. Similarly, palmitoylated proteins show affinity for highly curved

membranes[46]. To determine if this is a universal occurrence for any disordered, anchored, or denatured protein requires further experimentation.

Figure 14 reveals that mCRP readily binds curved membranes, much more so than pCRP, which hardly binds at all. Regions of curved membranes are thought to differ from flat regions in the way that lipids are packed. Curved regions have defect sites – sites where there is more space between headgroups than tails – which are thought to allow exposure of the hydrophobic tails to the surrounding aqueous solution. Defect sites are places on a membrane where protein and lipids can accumulate if there is a need for hydrophobic interactions. Modified CRP, which is stabilized by SDS, likely has hydrophobic portions exposed. Research demonstrates that mCRP likes to aggregate[47] which usually occurs through hydrophobic interactions. Here, hydrophobic regions could be stabilized by binding to defect sites, as observed by the high binding of mCRP, but not pCRP to curvatures of 100 nm.

2.3.6 Lysophosphatidylcholine (lysoPC) increases CRP binding to curved membranes

The presence of lysoPC has long been known to enhance CRP binding to damaged cell surfaces or on the surfaces of liposomes[48] . To investigate how changes in the chemical composition affect CRP binding, supported lipid bilayers that contained 3% lysoPC, 2% MB-DHPE (to measure fluidity) and 95% POPC were created over a nanopatterned surface where both flat and curved membrane regions were measured simultaneously. Upon the addition of lysoPC, the Pearson's correlation coefficient increased for both pCRP and mCRP Figure 17 A, B. In both cases, there is an increase in the distribution at larger coefficients. In Figure 18, the average correlation coefficient is

shown relative to random positions and a dashed line indicates the position without lysoPC. There is an increase by approximately 0.1 for both forms of CRP suggesting the lysoPC enhances binding to curved regions.

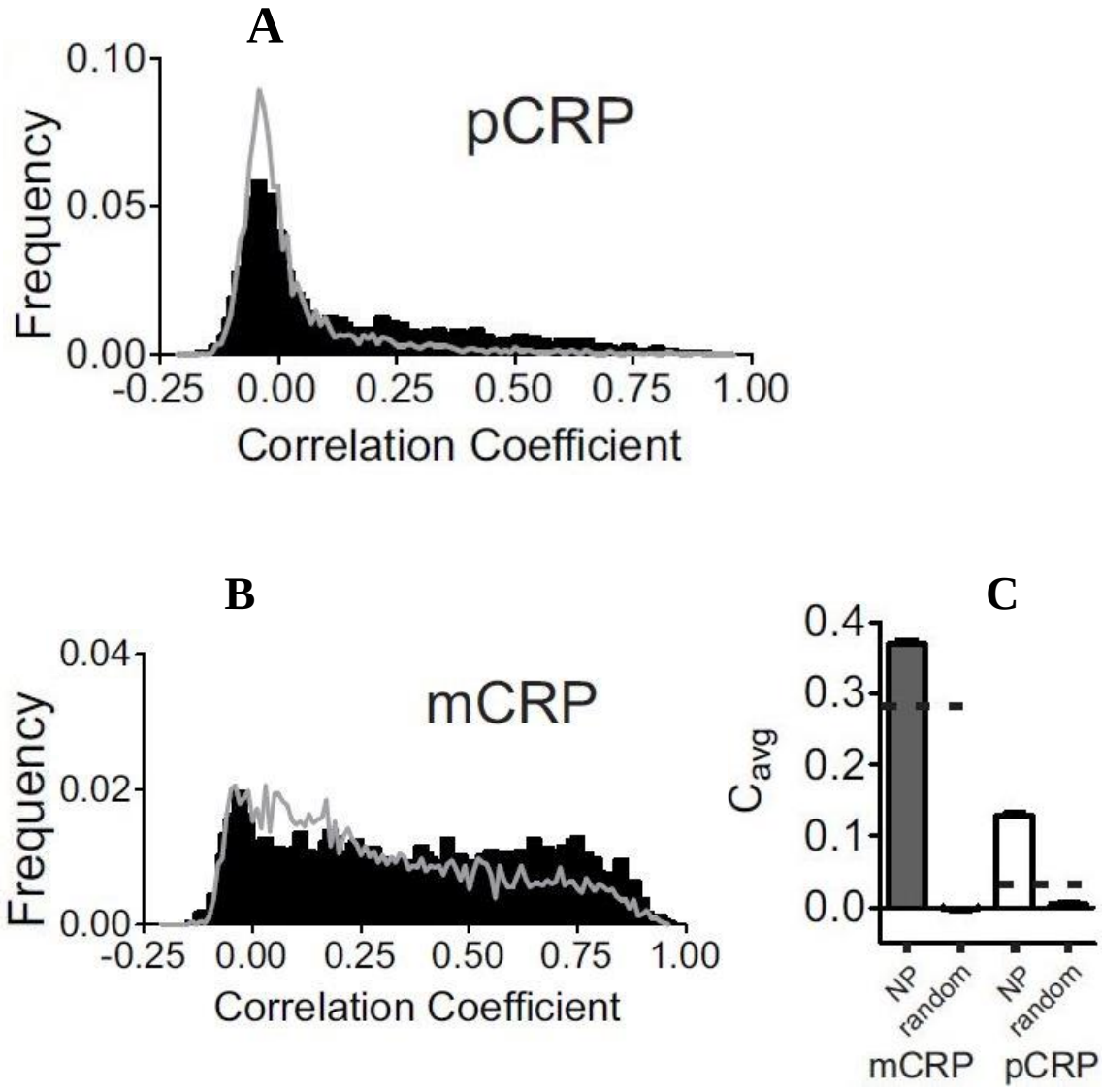

Figure 17. Lipid composition effects
CRP was incubated with lysoPC containing membranes (LysoPC:POPC:MB-DHPE at 3:95:2 molar ratio) that had regions of curvature (ROC = 55 nm). CRP (m and p conformers) were incubated with the bilayers for one hour at 37°C and then imaged. Images were cropped about nanoparticle positions and random positions and quantification is described in Figure 12. From cropped images, the Pearson's correlation coefficient was calculated for A) pCRP (black bars) and B) mCRP (black bars). The grey line in both plots denotes the distribution of the correlation coefficient in membranes that do not contain lysoPC. C) The average value of the distribution with SEM. The dashed line shows the average value when lysoPC is not in the membrane.

To determine how much CRP accumulates at nanoparticle regions when lysoPC is present, the intensity of CRP fluorescence is quantified .The height of the radial plot of mCRP increases slightly as shown in Figure 18, where the black line is the radial plot without lysoPC and the black circles are with lysoPC. The height of the radial plot of pCRP at nanoparticles increases more, from 97 counts to 438 counts, where the grey line is the radial plot of pCRP without lysoPC and the open circles depict the radial plot in the presence of lysoPC.

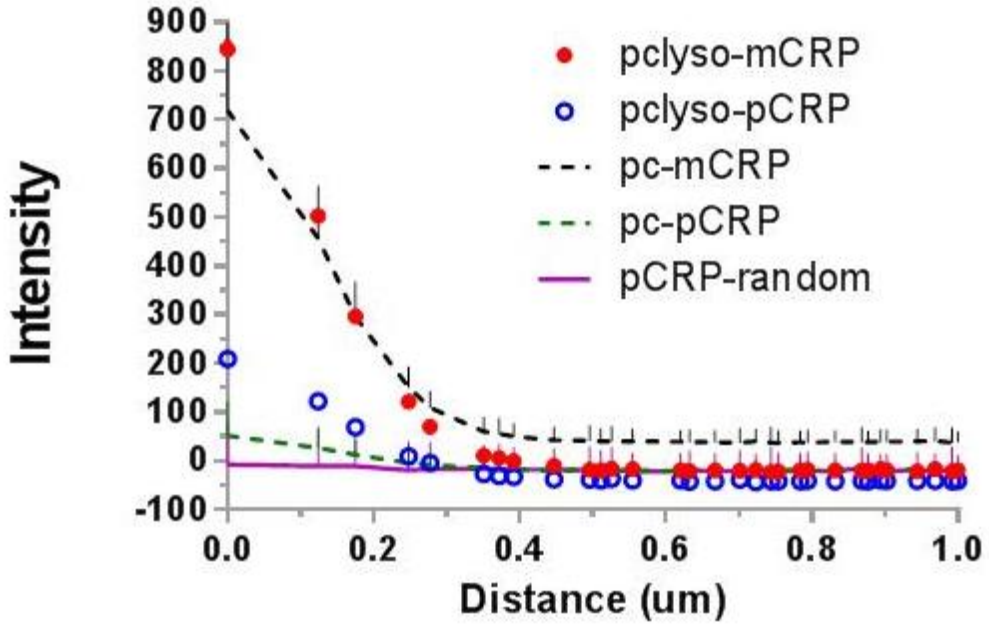

Figure 18. Radial averages of mCRP and pCRP binding to sites of curvature. mCRP and pCRP binding to lysoPC bilayers (red circles and blue circles, respectively), mCRP (black dashed line) and pCRP (green dashed line) on bilayers without lysoPC. The purple solid line is from random positions. Background intensity was subtracted using the average intensity of the tail from the CRP monoclonal C6 antibody radial plot. The error is SEM.

The increase of fluorescence at nanoparticle sites (ΔF) also shows that pCRP binding is affected by the presence of lysoPC as shown in Figure 19. Both the pCRP and the mCRP changes are statistically significant ($P < 0.05$), indicating that lysoPC serves to increase binding of all forms of CRP to curved regions more so than to flat regions, but affecting pCRP more than mCRP.

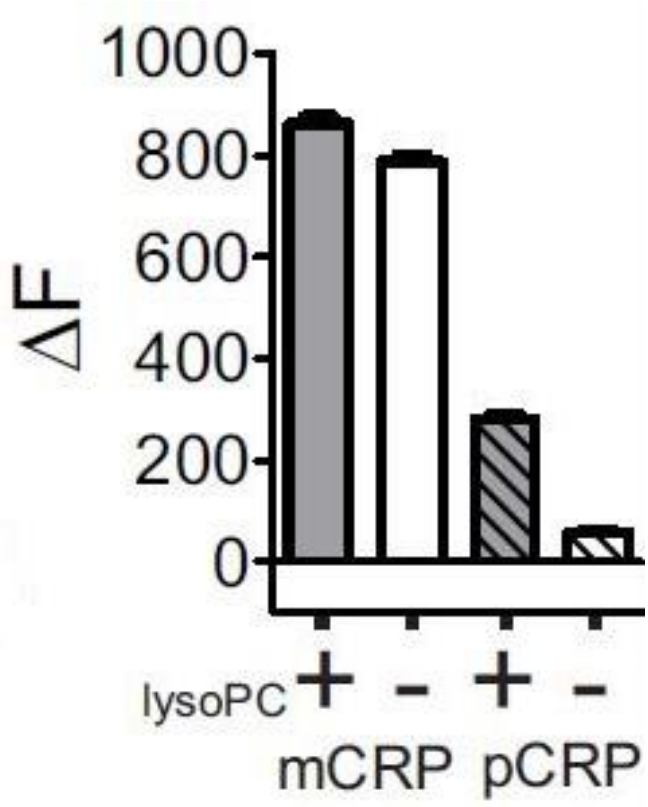

Figure 19. The average of the ΔF distribution.
ΔF for mCRP and pCRP with and without lysoPC at ROC 55nm. , ΔF, is calculated from radial plots and the average of the distribution is shown. In all bar graphs, the error is the SEM.

The data indicated that the lipid composition also affects binding to both curved and flat membranes. LysoPC is a marker for damaged membranes and the interaction between CRP and lysoPC was first identified in the 1970s[18]. One advantage of the experimental configuration is the ease at which lipid composition can be altered separately from the membrane shape. In Figure 17, we show that lysoPC enhances binding more at curved regions than on flat regions and enhances both pCRP and mCRP binding. This is likely due to the accumulation of single tailed lipids at sites of curvature[35]; there is a higher density of lysoPC at the curved regions to bind CRP. Others have suggested that lysoPC introduces irregularities into artificial lipid bilayers[18]and that these are essential to binding pCRP. The presence of lysoPC affects pCRP more than mCRP, increasing the accumulation by 4-fold as opposed to a 10% increase at curved membranes Figure 19, suggesting that mCRP associates in a way that does not depend significantly on binding lysoPC, whereas pCRP association does. pCRP likely interacts through headgroup interactions as others have observed on highly curved membranes lacking lysoPC[21].

2.3.7 Membrane shape affects CRP binding

The shape of a membrane has been shown to affect protein binding for a variety of membrane associated proteins, such as BAR domains[49], amphipathic helices[50], [51], and lipid –anchored proteins[46], [52]. By decreasing the size of nanoparticles used as a template for the supported lipid bilayer, higher curvatures (Rc = 27 nm) were examined.

Figure 20 shows how the Pearson's correlation coefficient distribution is affected by membrane shape for both conformations. The distribution shifted to higher, more colocalized coefficients for pCRP Figure 20A, whereas the shift was to lower coefficients for mCRP Figure 20B. In both figures the correlation coefficient between larger nanoparticles and CRP is shown as a magenta curve and the correlation coefficient distribution for smaller nanoparticles and CRP is shown as a bar graph.

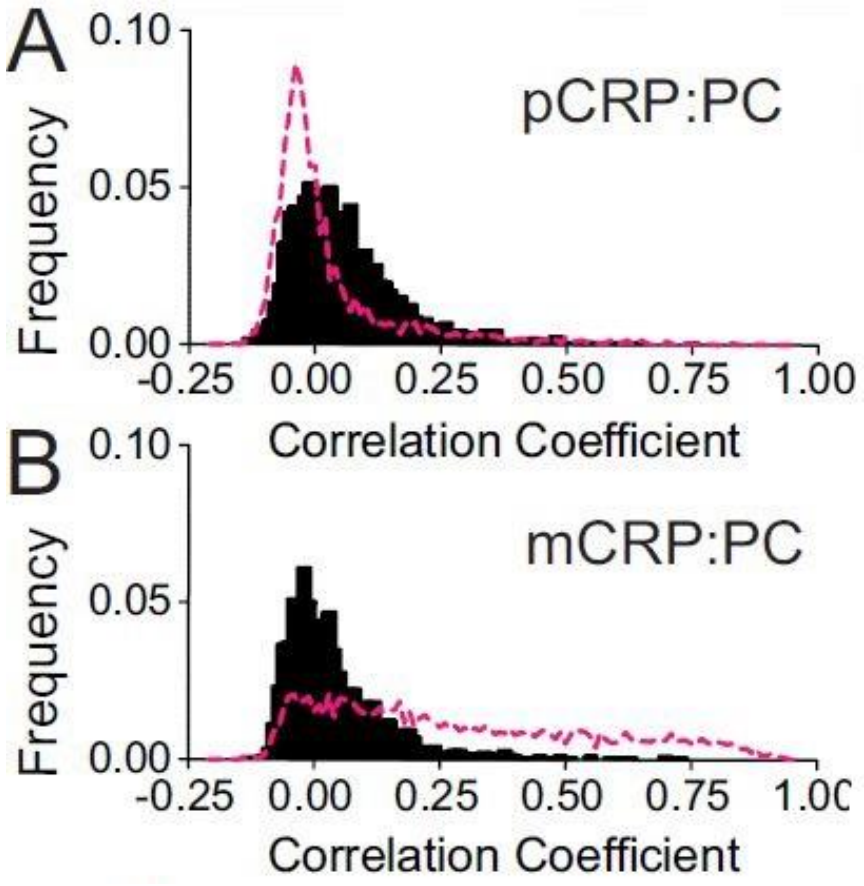

Figure 20. Membrane curvature effects:
CRP recruitment to curvature with a smaller nanoparticle support (d = 45 nm, ROC = 27 nm) was measured using confocal microscopy. Lipid bilayers contained 98% POPC, 2% MB-DHPE A) The Pearson's correlation coefficient distribution for pCRP and nanoparticle images, depicting the higher curvature (ROC = 25 nm, black bars) and lower curvature (ROC = 55 nm, magenta curve) normalized correlation coefficient distribution for 1574 and 3297 nanoparticle positions, respectively. B) The Pearson's correlation coefficient distribution for mCRP and nanoparticle images, depicting the higher curvature (ROC = 27 nm, black bars) and lower curvature (ROC = 55 nm, magenta curve) normalized correlation coefficient distribution for 1368 and 3792 nanoparticle positions, respectively.

The results were similar when 3% lysoPC was included in the bilayer Figure 21. mCRP does not select for higher curvatures nearly as well as lower curvatures, however

pCRP associates with higher curvatures better. The mechanism by which mCRP and pCRP interact with membranes is likely different.

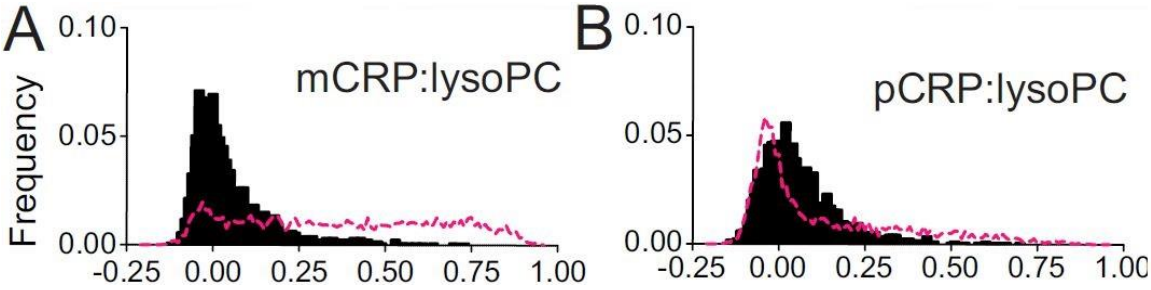

Figure 21. CRP recruitment to curvature:
CRP recruitment to curvature with a smaller nanoparticle support (d = 45 nm, ROC = 25 nm) was measured using confocal microscopy. Lipid bilayers contained 95% POPC, 3% LysoPC, 2% MB-DHPE A) The Pearson's correlation coefficient distribution for pCRP and nanoparticle images, depicting the higher curvature (ROC = 25 nm, black bars) and lower curvature (ROC = 55 nm, magenta curve) normalized correlation coefficient distribution. B) The Pearson's correlation coefficient distribution for mCRP and nanoparticle images, depicting the higher curvature (ROC = 27 nm, black bars) and lower curvature (ROC = 55 nm, magenta curve) normalized correlation coefficient distribution.

One key difference in the membranes that are formed over large nanoparticles (lower curvatures) compared to smaller nanoparticles (higher curvatures) is the surface area. When projected onto a 2D image, the larger nanoparticles contain 4.84 times the amount of surface area than a flat region and the smaller nanoparticles contain 2 times the amount of surface area (see Materials and Methods for the explanation). It is relatively straightforward to correct for the surface area differences when measuring intensity

Figure 22. The intensity (y-axis) was corrected for surface area by dividing by either 4.84 for low curvature membranes or 2 for high curvature membranes. After measuring the surface area corrected increase in intensity at curvature compared to flat

areas (ΔF_{SA}), mCRP collects at larger nanoparticles (lower curvature) at a density greater than the accumulation at smaller nanoparticles (higher curvature). However, pCRP shows the opposite trend, in agreement with the work of others[21]. The shape of a membrane clearly affects CRP binding and this depends on the form of CRP.

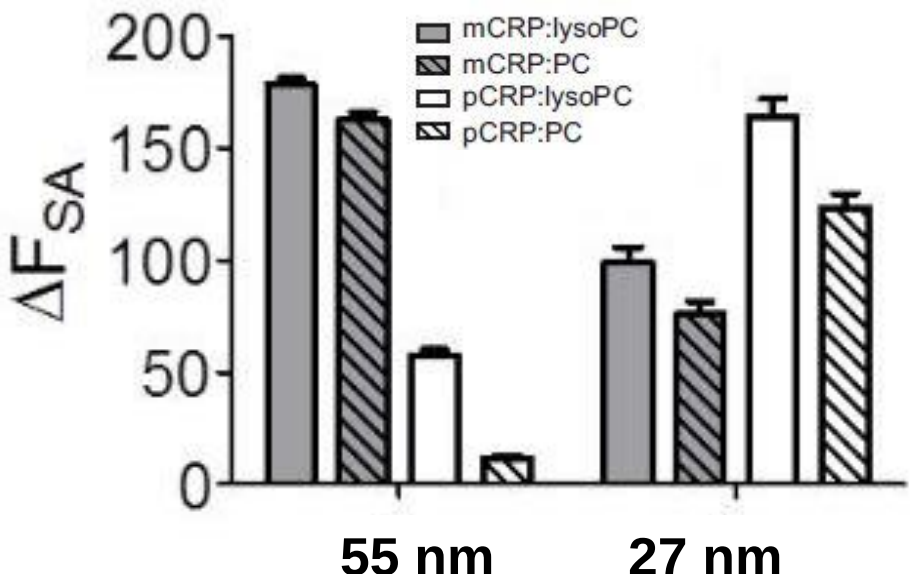

Figure 22. The preference for curvature over flat regions (ΔFSA).
ΔFSA is calculated from radial plots (not shown) and normalized for differences in surface area. The mean +/- SEM are plotted for all lipid, curvature and CRP conformation. To correct for surface area differences, the values for higher curvature were divided by two and the values for lower curvature were divided by 4.84 to compare the protein density at curvature to that at flat regions. Grey columns correspond to mCRP, white columns are pCRP. Striped columns contain no lysoPC, whereas the solid columns contain 3% lysoPC. Antibodies used for these experiments were CRP monoclonal C6 and CRP monoclonal D7 for curvatures with radii of 55 nm and 27 nm, respectively. A supplemental figure with dot blots for these antibodies can be found in the appendix.

The native form of CRP (pCRP) binds at a higher density to higher curvatures than to lower curvatures both in the presence of lysoPC and without lysoPC in *Figure 22*. This is in agreement with past work on CRP[21] and other proteins, such as palmitoylated proteins[46], [52] and amphipathic helices[50]. In previous work on CRP, very high curvatures (ROC = 10-15 nm) were tested and shown to bind pCRP better than lower curvatures (ROC = 20-35 nm), however the lower curvatures likely bound pCRP to a lesser extent based on the fact that CRP was activated in some way to be able to bind

C1q after incubation[21]. All binding was Ca^{2+}-dependent, indicating that the pCRP:PC interaction was likely through binding of the PC moiety as opposed to an interaction with the lipid tails. Curvature could enhance binding by facilitating multivalent interactions[53] .To support this mechanism, recent work measured CRP binding constants on an engineered surface where the distance between PC ligands was varied[54]. In this work, the dissociation constant decreases by approximately 25-50% when PC is separated by 1.0-2.0 molecules/nm^2, a distance larger than the natural packing of lipids on a flat membranes[55].Once PC groups are too far apart for multivalent binding (>2.0 molecules/nm^2), the dissociation constant increases again. Regions of curved membranes are thought to differ from flat regions in the way that lipids are packed and curving a bilayer would results in a larger spacing between lipid head groups, also known as defect sites.

At lower curvatures (ROC = 55 nm) mCRP bound membranes significantly more than pCRP. Other proteins, such as amphipathic helices, preferentially insert into curved membranes through hydrophobic interactions with the defect sites that occur as a lipid membrane bends around a curved surface [52]. Curved regions have defect sites, which are thought to allow exposure of the hydrophobic tails to the surrounding aqueous solution and potentially interact with hydrophobic proteins.

Defect site binding to membranes, alone, cannot explain the clear preference mCRP has for larger curvatures

Figure 22. One mechanism by which a *specific* shape preference comes about is from a 3D protein structure that has an intrinsic curvature, like a BAR domain[49] or a clathrin coated pit[34]. These larger structures then prefer lipid membranes that match in

shape to their intrinsic curvature. It is possible that mCRP could form larger aggregates on membranes, as others have proposed[47], giving rise to a larger structure that has a specific curvature preference. We see no direct evidence of aggregation in our assay. A second mechanism for *specific* curvature sensing could arise from multivalent binding. Recent work shows that CRP binds with different affinities based on the separation of PC headgroups[54]. For a protein to detect curvature in this way would depend on retaining some multimeric state. It is possible that higher order structures are what drive CRP binding and this structures form better on membranes with a radius of curvature of 55 nm as opposed to 25 nm. In the future, a wider spectrum of sizes could be studied to further understand CRP binding.

2.4 Conclusion

In this Chapter, a nanopatterned substrate was utilized to introduce curvature into continuous lipid bilayers for quantitative image analysis of CRP binding. One major advantage of this assay is the ability to separately tune chemical composition and membrane shape[35]. This work demonstrates that the conformational state of CRP affects lipid binding. Monomeric CRP readily associates with membranes, favoring sites of curvature over flat regions. Native, pCRP does not easily associate with membranes until the curvature is high (ROC = 25 nm) or until lysoPC is introduced. CRP likely recognizes damaged lipidic materials through a mechanism that combines PC binding by pCRP and membrane insertion into defect sites, which stabilizes mCRP. Both of these types of interactions are strengthened at sites of curvature.

CHAPTER THREE

3.1 CRP recognition of apoptotic cellular membranes

CRP is known to bind to apoptotic cells to facilitate their clearance[56], and this activity prevents autoimmune disease[57]. To do this, a possible conversion takes place between two isoforms – pentameric CRP and modified CRP. This conversion affects CRP binding to C1q, an established recognition protein of the innate immune system. However, the triggers that cause pentameric CRP (pCRP) to convert to the modified form (mCRP) upon binding to apoptotic cells is still not well understood[7],[19]. Moreover, the factors that allow CRP to recognize and bind PC in apoptotic cells selectively compared to healthy cells need to be established. Since both healthy and apoptotic cells have PC on their outer leaflet, it is probable that another factor that helps CRP bind to apoptotic cells. There are several differences between apoptotic and healthy cells. First, the physical structure of the cell membrane varies as the apoptotic cells form cellular blebs (curved protrusions) during apoptosis. Second, the distribution of lipid compositions between the inner and outer leaflet of cell membrane is changed since the phosphatidylserine (PS) flip to the outer leaflet during apoptosis[58].

We hypothesize that once CRP binds to the surface of apoptotic cells conformational changes can take place that activate CRP-C1q binding. To test our hypothesis we quantitatively measured CRP binding to apoptotic cells versus healthy cells.

For our *in vivo* work, we used MES-SA cells, a human uterus sarcoma cell line, to induce apoptosis using the drugs valinomycin and paclitaxel. After treatment, we measured the binding of CRP using fluorescence microscopy. The cells membrane was visualized using Annexin V, which binds to the phosphatidylserine present on the extracellular side of the apoptotic membranes, and large blebs were identified by their shape. This work included three stages, one where we measured whether or not CRP binds more to apoptotic cells. Secondly, the binding of the C1q protein to apoptotic cells and the immunofluorescence of C1q with CRP on apoptotic cells were measured. The research has also advanced to examine the conversion of CRP from pentameric to monomeric form after incubation with apoptotic cells for different amounts of time by utilizing a RNA aptamer that specifically binds to mCRP but not pCRP[42], [59].

3.1.1 Apoptosis

Apoptosis is programmed cell death accompanied by morphological changes such as cell shrinkage, chromatin condensation, and plasma membrane blebbing. Later, these blebs separate from the dying cells as apoptotic bodies with their membranes intact and then they are engulfed by macrophages[60]. Apoptosis differs from necrosis since necrotic cells do not form blebs, and do lose their membrane integrity. This process starts with the cytoplasm swelling and ends with cell lysis when cells release their intracellular components that stimulate inflammation[61].

Another important feature of apoptosis is the flipping PS to the outer leaflet of the plasma membrane, which is considered as a recognition ligand for neighboring cells. This results in a quick phagocytosis to prevent inflammation. The fast uptake and removal of

these cells with no release to their constituents leads to no inflammatory response[60]. Also, apoptotic cells can stimulate phagocytes to produce anti-inflammatory cytokines.

The mechanism by which PS translocate to the outer leaflet of the membrane is not completely understood. Lipid asymmetry under normal conditions is maintained by the activity of flippases and floppases between the outer and inner leaflet. However, during apoptosis scramblase becomes activated which leads to loss lipid asymmetry and causes PS to expose to the outer leaflet. Apotosis can also be detected by some proteins such as AnnexinV which is shown to be exposed on the surface of apoptotic cells. Annexin V, is a specific protein binds strongly to PS and helps to detect apoptosis[58].

In addition to PS flipping to the plasma membrane outer leaflet, the lipid compositions of this outer leaflet also undergo specific changes during apoptosis. It has been shown that the lipid order of the outer leaflet significantly changes during apoptosis. The loss of lipid order has been connected with lipid scrambling and sphingomyelin (SM) hydrolysis which cause SM to flux from outer to inner leaflet[62]. Apoptosis is initiated through complicated, regulated machinery by activating Caspases, proteins degradation enzymes.

3.1.2 Drugs used for Apoptosis

In this study, two different drugs, valinomycin and paclitaxel were used to induce apoptosis. The first, valinomycin is a selective membrane transporter protein for potassium ion K^+ across the cell membranes. It is a cyclic antibiotic consists of 12 carbonyl groups allows it to bind to metal ions and solvates in a polar environment. Valinomycin captures K^+ to its inner cavity and form complex. It also has isopropyl groups and methyl groups

responsible for its solvation in non-polar environment. Therefore, in the membrane lipid phase valinomycin complexed with K^+ can be transferred into the other side of the cell[63]. It has been reported that valinomycin triggers mitochondrial permeability transition causes intracellular acidification which activates cysteine active site protease causes degradation of the nuclear proteins and chromatin condensation[64]

3.1.3 Paclitaxel (Taxol)

Paclitaxel is a chemotherapy drug that binds tubulin and protects microtubulin from being disassembled by stabilizing them, and blocks G_2/M phase in cell cycle[65]. The mechanism by which Taxol induces apoptosis is still not very clear. It has been reported that Taxol induced massive apoptosis in MCF7cells[66]. Taxol has been shown to modulate the phosphorylation of some molecules and cycles in MCF7 cells that are involved in apoptosis and cell proliferation. The significant elevation in the activities of these molecules, ERK and p38 MAPK in cells treated with Taxol, leads to the suggestion that these molecules mediated Taxol induced apoptosis in MCF7 cells. Previous studies reported that ERK promotes apoptosis by inducing the release of cytochrome C which enhances the activation of Caspases involved in apoptosis[67].

3.1.4 CRP binds to apoptotic cells and converts to mCRP

CRP has been shown to bind to apoptotic cells and consequently enhances the activation of the classical complement pathway. It also promotes their opsonization and phagocytosis by macrophages[56]. CRP could target many molecules on the surface of apoptotic cells such as PC head groups, lysoPC, ox PC, and FcγRIII. Studies have also

shown the binding of CRP to the membranes of cells or liposome will result in a rapid but partial structural change of pCRP producing a hybrid molecule, membrane bound molecule ($mCRP_m$), and that retains a pentameric conformation with partial structural changes[19]. $mCRP_m$ binds to C1q and leads to complement activation.

Research suggests that mCRP has a proinflamatory effect since it was bound to membranes in atherosclerotic plaques, however healthy vessels have neither form of CRP [6]. mCRP- HAECs interaction was mediated by mCRP insertion to the membrane[68]. The nature of this binding was evaluated by washing the cells with high salt, acid, or base to dissociate electrostatic adsorption, high affinity receptor binding, or peripheral protein from cell membrane, respectively. mCRP interaction with HAECs was not affected by any of these treatments. This indicated that mCRP binding was receptor independent and likely driven by lipid interactions.

mCRP has been shown to bind to lipid raft microdomains in human aortic endothelial cells (HAECs) with a binding affinity 20x more than pCRP[68]. This interaction was mediated by mCRP membrane insertion instead of receptor binding using the putative cholesterol binding sequence of CRP (aa 35-47) and the C-terminal octapeptide (aa 199-206). This was characterized by pre incubation of mCRP with 3H12, antibody that recognizes (aa 199-206) or with 8C10, antibody that recognizes (aa22-45) which contains cholesterol recognition domain. Then mCRP complexed with the antibody was injected under monolayer contains egg PC/cholesterol/SM (3:1:1) or egg PC monolayer that does not contain cholesterol. Results from pressure measurements indicate that mCRP complexed with 3H12 decreases binding of mCRP to the monolayer with cholesterol by 60%, while 8C10 decreased by 40%.

In addition to the proinflamatory effect, mCRP has showed to play dual role in activation and inhibition of the classical complement pathway. mCRP binds to C1q, the initiator of the classical complement pathway, on the damaged human cells surface and necrotic heart tissue. This leads to trigger the activation of the complement pathway and allows opsonization with C3b. C4bp, a regulator and classical pathway inhibitor, and factor H, the alternative pathway inhibitor, were recruited to the damaged cells surfaces by mCRP which leads to block the complement cascade progression and inhibit the inflammation[69].

3.2 Material and Methods

3.2.1 Induction of apoptosis and CRP incubation

MES-SA cells were grown at 37°C / 5% CO2 in McCoy's media supplemented with 10% fetal calf serum, 100 μg/mL penicillin, and 100 μg/mL streptomycin. Cells were incubated in DMSO or 100 μM valinomycin for 4 hrs. Hoechst 387 DAPI nuclear stain was added to the cells and allowed to incubate for 5 minutes at 37°C. Then, cells was incubated with Annexin V Alexa594 stain for 15 minutes at 37°C. Cells were fixed by using 4% formaldehyde for 15 minutes and then washed 3 times with phosphate buffered saline PBS buffer. Human CRP was purified from endotoxin by using Endotoxin Removal Gel. 20 μg/mL CRP was added to both fixed control and apoptotic cells and allowed to incubate for 45 minutes in the presence of Tris buffer with 1 mg/mL BSA. Primary anti-CRP (C8), mouse IgG monoclonal (1:100000) (Santa Cruz) was incubated for 20 minutes, then secondary goat anti-mouse immunoglobulin G with Alexa-488 (1:100000) (Life Technologies, A 11005) were incubated for 20 minutes.

Images were taken using an Olympus laser scanning confocal microscope. The membrane of each individual cell was highlighted using free hand tool, then the intensity of CRP was calculated by using this equation:

$$CRP\ Intensity = CRP\ Integrated\ Density\ of\ Cell\ Area - (Mean\ Background\ Intensity \times Cell\ Area) \quad \textit{Equation 5}$$

3.2.2 Induction of apoptosis and C1q incubation

100 μM valinomycin dissolved in DMSO was used to induce apoptosis in MES-SA cells for 4 hours. Control cells were exposed to an equal concentration of DMSO (1:1000). Cells are then stained with cell mask in PBS buffer followed by the addition of 10 μg/mL Hoechst DAPI nuclear stain (Invitrogen), and incubated for 5 minutes at 37^0C. Cells were washed by PBS, and fixed by incubation with 4.0% formaldehyde for an hour followed by washing three times with PBS. The apoptotic and control fixed cells were incubated with C1q (10 μg/mL) for 30 minutes at 4^0C. C1q was visualized using a primary mouse monoclonal anti-C1q (ab714940) antibody and a secondary rabbit anti-mouse IgG Alexa 488 with a 1:1000 dilution.

3.2.3 Induction of apoptosis by using paclitaxel

Paclitaxel was diluted with DMSO to final concentrations of 700 nM or 900 nM. Cells were incubated for 16 hours, and then stained with DAPI and annexin V Alexa594. Control cells were exposed to DMSO with a final dilution (7:10,000) or (9: 10,000). Live Cells were imaged using confocal microscopy.

3.2.4 Aptamer detection of CRP conversion

MES-SA cells were incubated in 900 nM of paclitaxel for 16 hours. Afterward, cells were washed 3 times with PBS buffer. 10 µg/mL of CRP or 10 µg/mL of mCRP were added to apoptotic cells which had been plated in different wells at varying incubation times. Protein incubation was done with Tris buffer with 1% BSA to block nonspecific binding. mCRP was prepared by heating pCRP with 0.01% SDS at 80^0C for an hour. A RNA aptamer specific for mCRP (Integrated DNA Technologies, Coralville, IA) and end labeled with Cy3 was reconstituted with DEPC treated water and stored at -20^0C until use. The RNA sequence was 5′-Cy3-GCC UGU AAG GUG GUC GGU GUG GCG AGU GUG UUA GGA GAG AUU GC- 3′. Next, cells were washed with PBS to remove unbound proteins and then stained with DAPI stain followed by a 30 minute incubation with the aptamer at room temperature. Finally, cells were washed with PBS before imaging by confocal microscopy. Images were analyzed using ImageJ as shown in Figure 27.

3.3 Determining incubation time for apoptosis

3.3.1 Visualization apoptotic MES-SA cells using Annexin V

Annexin V Alexa 594 is a protein that has high affinity to bind to phosphatidylserine that flips to the outer leaflet of the plasma membrane upon programmed cell death. This assay allows to visualize the membrane of the apoptotic cells, blebs and quantify the percentage of apoptosis. Cells treated with 900 nM paclitaxel overnight show higher binding to Annexin V Alexa 594 than cells incubated with 700 nM of the drug (Figure 23). By counting the cells that were stained by annexin V Alexa594,

the percentage of apoptosis of the cells incubated with 900 nM paclitaxel was 27.0%±4.24 (SEM) as compared with the 700 nM apoptotic cells which was 21.4%±3.37 (SEM) (Figure 23).

A.

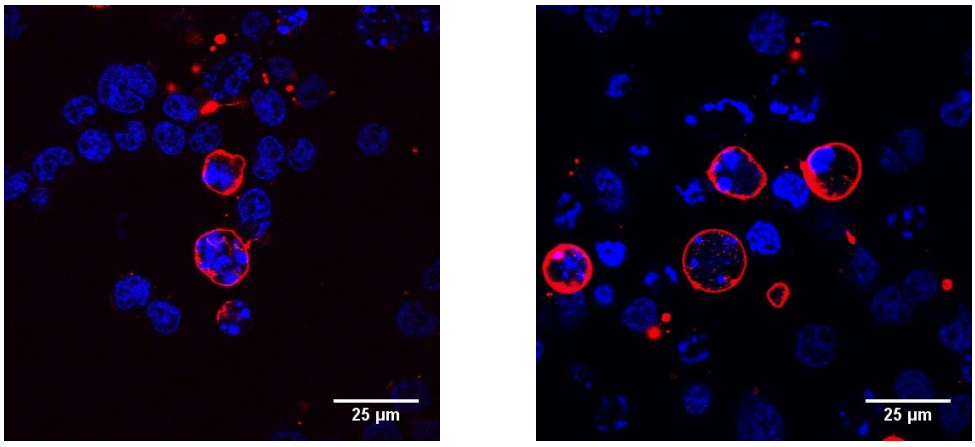

700nM Paclitaxel **900nM Paclitaxel**

B.

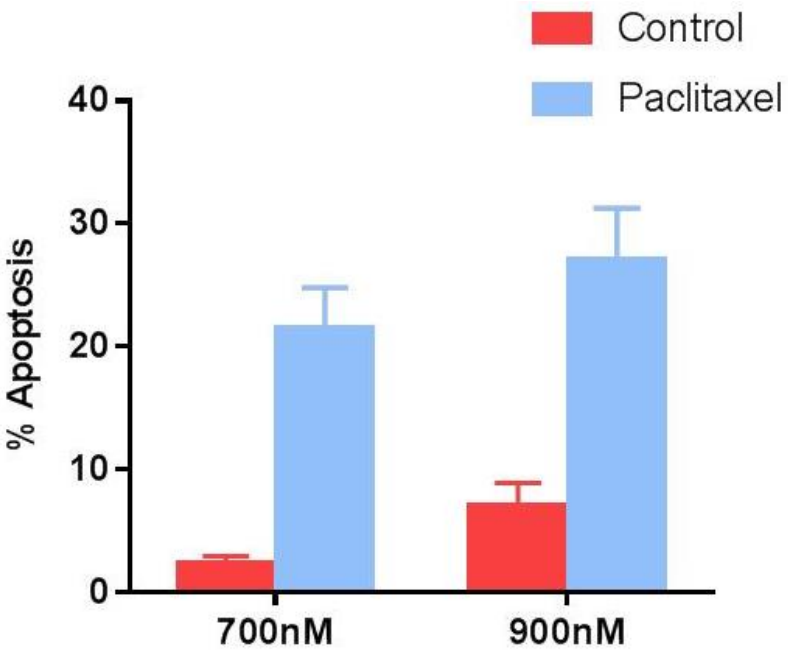

Figure 23. Annexin V Alexa 594 binds to apoptotic cells.
Annexin V Alexa 594 binds to phosphatidylserine (PS) in live apoptotic cells (red). A) Fluorescent images of annexin V binding to cells after treatment with paclitaxel overnight. B) Percentage of apoptosis was measured by counting the cells that positively stained with Annexin V. N=453 and 500 cells for control groups treated with 700nM and 900nM, respectively. For Paclitaxel groups, N=557 and 406 cells for cells treated with 700nM and 900nM, respectively.

3.3.2 CRP binding to apoptotic cells

After exposing MES-SA cells to valinomycin, quantitative measurements of CRP binding to the cellular membrane was done using ImageJ. The free hand tool in image J was used to highlight the outline of the cells' membranes and to measure the intensity of CRP binding to each individual cell. Blebs of various curvatures can be seen in the apoptotic cell. The percentage of the apoptotic cells was 30% as compared to the control cells which was 6%. This was calculated by counting the cells that were stained by Annexin V Alexa594. Using image J and a set of images, the average intensity of the CRP binding the control cells was measured to be (2,798) with the standard error (252.1). For the apoptotic cells, the average intensity was (4,089) and the standard error was (654.4). (Figure 24). The intensity of the CRP was calculated by the equation 5 above.

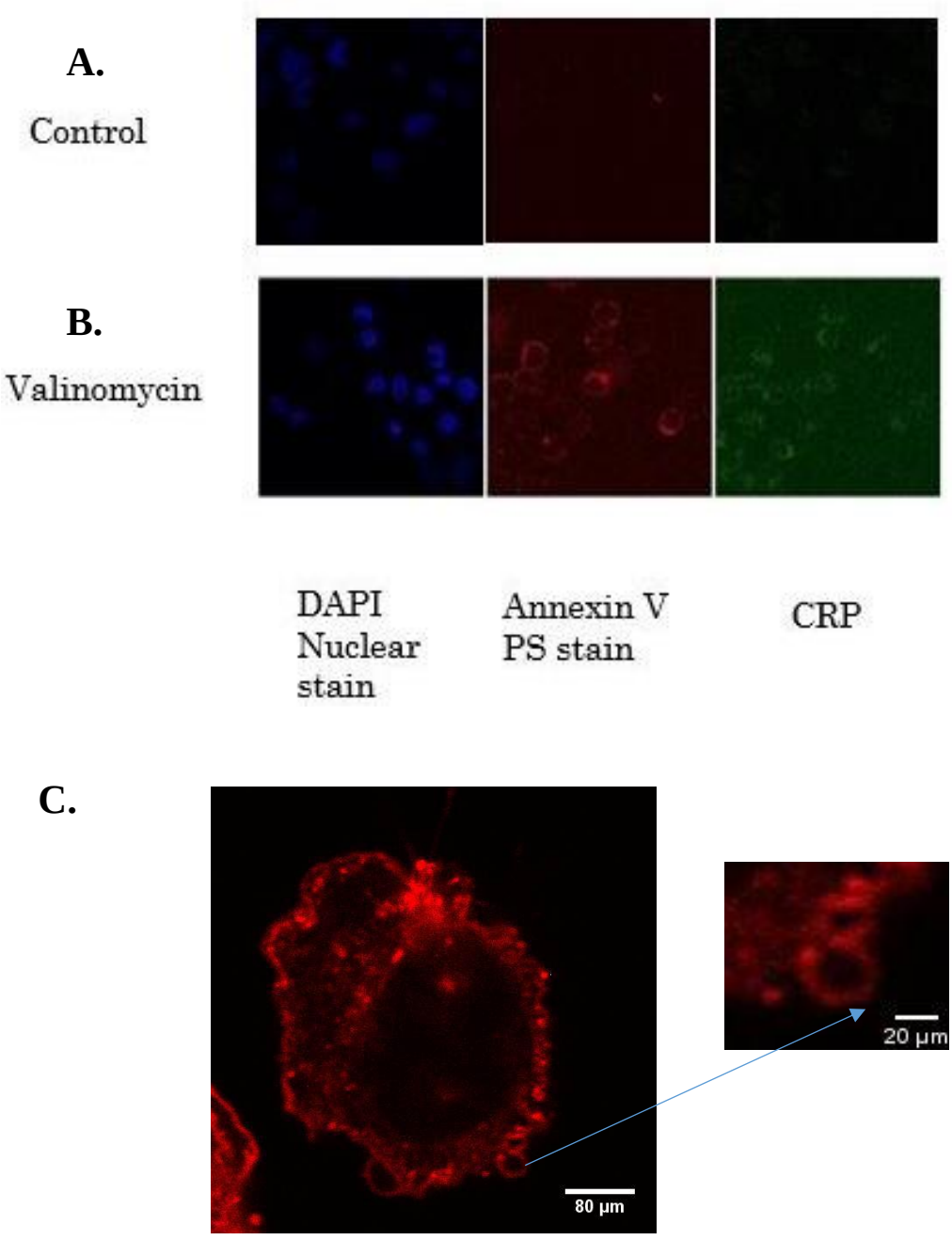

Figure 24. CRP binds to apoptotic fixed MES-SA cells.
A.) Control Cells treated with DMSO. B) Cells after incubating with Valinomycin for 4hours. C) Apoptotic cell with blebs. Cells were stained with Annexin V that binds PS on the outer leaflet of the cell membrane. Primary anti-CRP (C8), mouse IgG monoclonal was used. Images were taken using confocal microscopy. Image C was taken by Kathryn Palma.

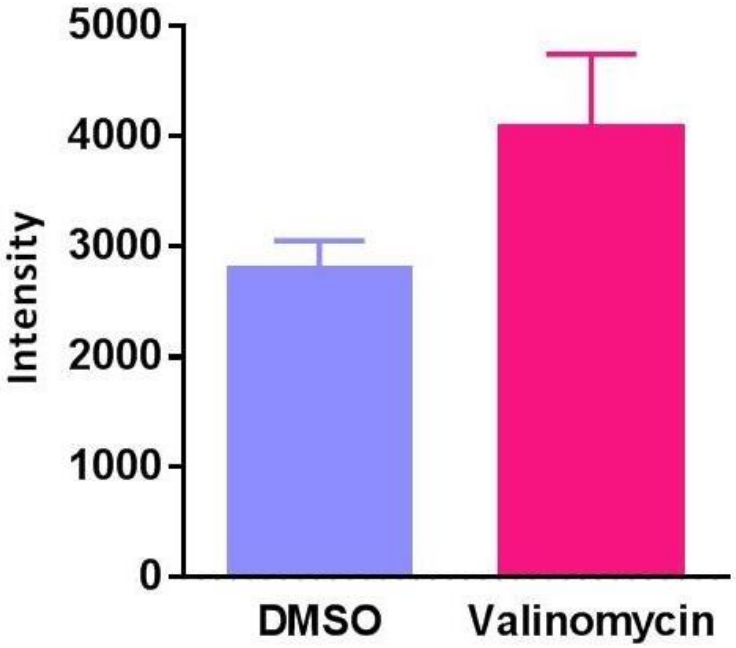

Figure 25. Intensity of CRP binding to control and apoptotic cells.
Average integrated Intensity of CRP binding to control and apoptotic cells. The antibody background integrated intensity and areas of images that have no cells were subtracted and calculated using (Eqn. 3). N= 103, 170 cells for control and apoptotic cells respectively. No statistical significance was observed between control and apoptotic cells using t-test. p=0.136.

3.3.3 C1q binding to apoptotic cells

C1q, an early component of the classical complement pathway, has been shown to bind to apoptotic cells and enhance their clearance by inducing the activation of the complement pathway[27]. Our goal is to characterize the interaction between apoptotic cells and C1q, and to quantitatively measure C1q binding to the apoptotic cells. C1q was incubated for 30 minutes at 4^0C after staining the cells with DAPI stain and then fixing the cells with 4% formaldehyde. C1q was visualized by using primary and secondary

antibodies. Images were acquired using confocal microscopy. Condensed apoptotic nuclei were visualized using DAPI nuclear stain, a commonly used assay to assess nuclear morphology[70]. Annexin V was not used to check for apoptosis due to its binding affinity to PS, which can compete for C1q binding. Area of each nucleus was obtained using the threshold tool in ImageJ to highlight the nucleus. The average from 3 days was used. The membrane of each individual cell was highlighted, and then the intensity of C1q was obtained using ImageJ and the (*Eqn. 3*) listed above.

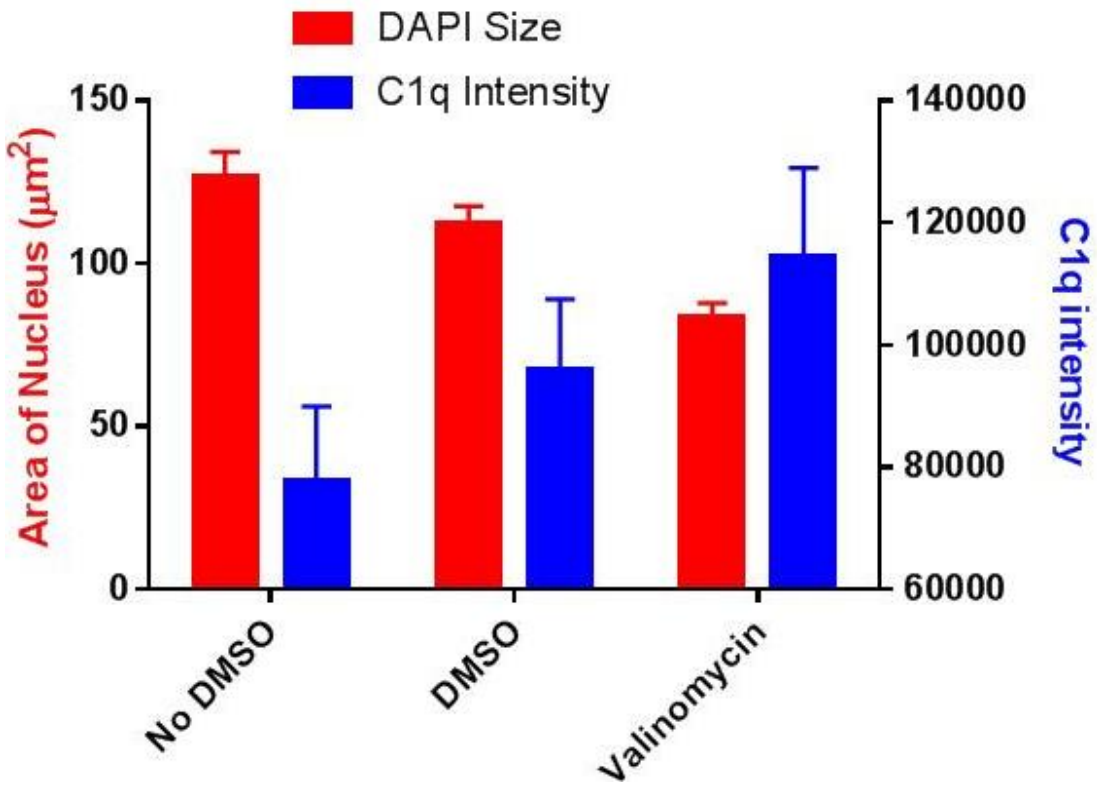

Figure 26. C1q binds to fixed apoptotic MES-SA cells.
The integrated intensity of C1q binding reflects the mean ± SE of three experiments. N= 47, 53, 44 cells for non-treated cells, cells treated with DMSO, and valinomycin respectively. The intensity of the background for each image was subtracted. Statistical significance was observed (P=0.022) between the average area of nuclei of cells treated with DMSO, and apoptotic cells. The average area of nuclei of cells treated with neither DMSO nor valinomycin was significantly less than average area of apoptotic cells (P=0.008). No statistical significance was observed of the average C1q intensity between control and apoptotic cells.

Cells treated with valinomycin are shown to decrease in the area of the nuclei as compared to the cells exposed to DMSO or cells treated with neither valinomycin nor DMSO. The average area of apoptotic cells' nuclei, DMSO treated cells 'nuclei, or the nuclei of cells not exposed to DMSO or valinomycin are 83.60±4.30, 112.44 ±5.28, and 128.46 ±7.98 respectively. The fluorescence integrated intensity of C1q increases when cells were apoptotic.

Quantitatively, the average intensity of C1q bound to apoptotic cells is 114497.80 ± 14516.46 whereas the cells treated with DMSO have less C1q bound to them as reflected by the fluorescence average intensity which is 95986.25 ± 11497.00. Untreated cells have less C1q bound to them with an average fluorescence intensity 77747.39 ± 1211.79.

3.3. Aptamer binds to apoptotic cells incubated with pCRP and mCRP over time

pCRP loses its pentameric structure and undergoes conformational rearrangement when it binds to endothelial cell membrane, forming mCRP that deposits in the blood vessel walls[23]. Our lab recently identified a RNA aptamer that binds specifically to mCRP but not pCRP[42]. In this research, aptamer was utilized to investigate whether the membrane of apoptotic cells can induce CRP conformational change. To follow the conversion from pentameric to monomeric form, CRP was incubated with the MES-SA apoptotic cells with different incubation time. The average intensity of aptamer binding to the membrane of apoptotic cells was determined by using ImageJ. The membrane of

each individual cell was highlighted, then the intensity of aptamer was calculated by using this equation:

$$Aptamer\ Intensity = Aptamer\ Integrated\ Density\ of\ Cell\ Area - (Mean\ Background\ Intensity \times Cell\ Area) \quad \textit{Equation 6}$$

The results show high aptamer binding intensity with the cells incubated with mCRP, while the cells incubated with pCRP show less binding (Table 1). Also, the results indicate higher intensity of aptamer binding to the cells incubated for two hours with pCRP as compared to the cells incubated for one hour.

A)

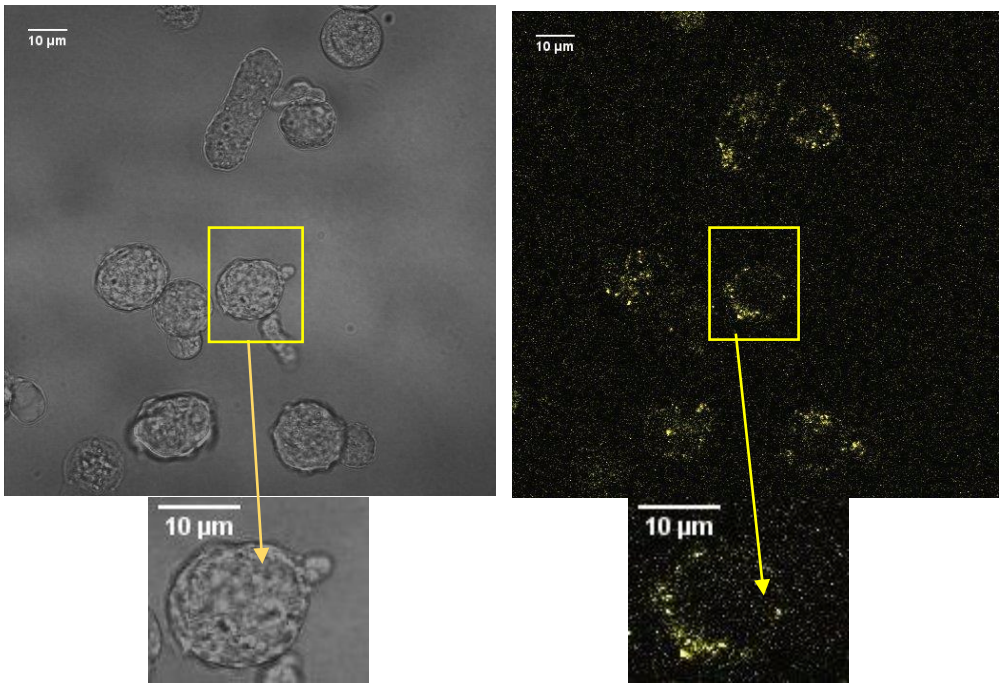

B)

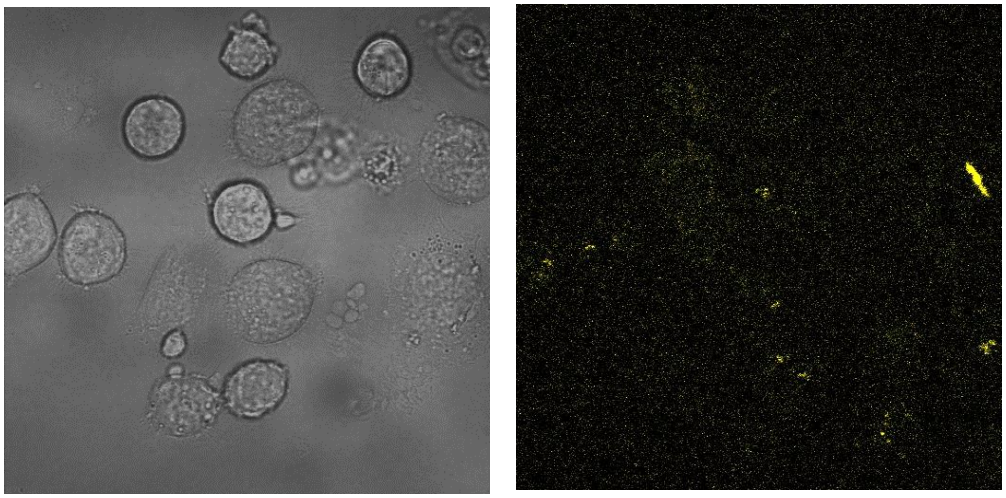

Figure continues on the next page.

C)

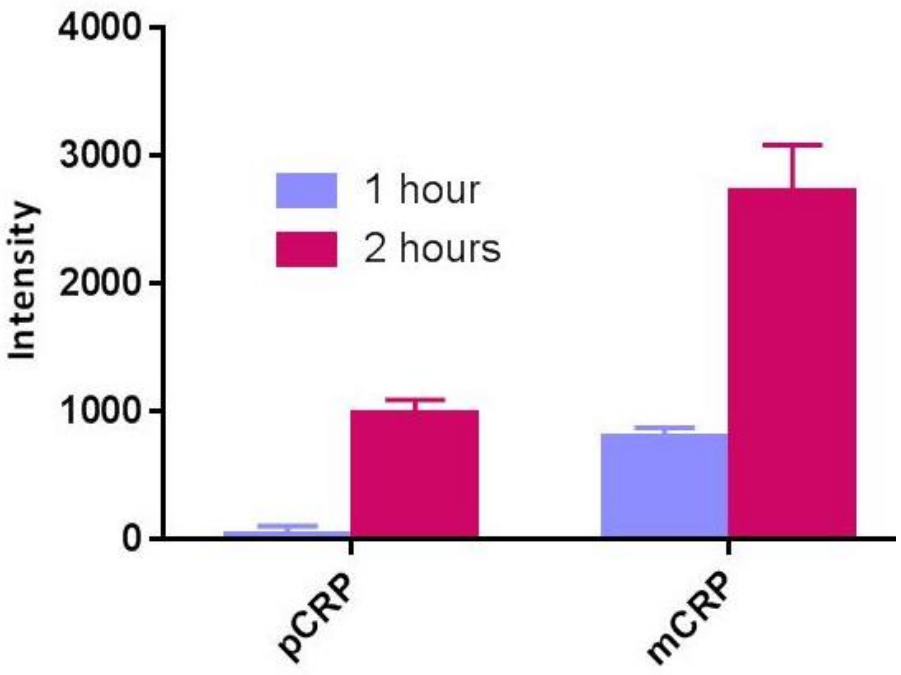

Figure 27. Aptamer binds to apoptotic cells at different time incubation.
A) Aptamer binds to apoptotic cells after incubating with mCRP for 2h, B) pCRP for 2h. C) Average integrated density of aptamer binds to apoptoic cells at varying incubation time with the antibody background intensity subtracted. Error bar is SEM. N=248,337 and 281, 364 for pCRP and mCRP at 2hrs, 1hr respectively. Statistical significance was observed ($p<0.0001$) between pCRP, mCRP treated cells.

3.4 Discussion

Due to the significant role of CRP and C1q in removing apoptotic cells and activating the complement system pathway, we aimed to quantitatively assess the binding of these proteins to apoptotic cells. The results revealed that CRP preferred to bind to apoptotic cells compared to control cells. Previous studies have confirmed colocalization of CRP on the apoptotic cell surface[19].

We also investigated whether the membrane of apoptotic cells induce pCRP structural changes to mCRP. A RNA aptamer that specifically binds to mCRP but not to

pCRP was utilized in this study to follow the pCRP conversion to mCRP on the surface of apoptotic cells membranes. The average intensity of aptamer that bound to cells incubated with mCRP was significantly higher ($p<0.0001$) than cells incubated with pCRP for two hours and one hour. Also, cells incubated with pCRP for two hours have showed significant aptamer binding than cells incubated with pCRP for one hour ($p<0.0001$). These data indicate that during two hours of incubation, more pCRP molecules dissociate to mCRP upon binding to the membrane of the apoptotic cells. Our finding is in agreement with previous work that showed the rapid dissociation of pCRP on the surface of apoptotic Jurkat T cells after 30 minutes of incubation by using mCRP mAB 3H12[19].

To further confirm our finding, future work can measure tryptophan fluorescence of CRP after varied incubation time with apoptotic cells by using the supernatant to detect conversion of pCRP to mCRP. However, separation would be extremely challenging. Due to CVD relevance, future work can focus on using Human Aortic Endothelial Cells (HAEC) to investigate if conditions for pCRP conversion is cell type specific or universal. Since previous studies suggested that binding pCRP to apoptotic cells is mediated by lysoPC[56], fluorescently tagged lysoPC and CRP can be used for colocalization analysis for imaging.

CHAPTER FOUR

4.1 Using fluorescence binding assays to characterize CRP conformational changes

4.1.1 Protein denaturation

Proteins in their native states have three dimensional folding structures known as secondary, tertiary, and quaternary structure. The proper function of a protein relies on its native form. Exposing a protein to any factor such as organic solvents, acids, bases and heat leads to the protein losing its native form and ability to perform its biological activity, and to protein denaturation. On the cellular level, denaturation of a protein causes disruption in the biological activity and cell death. Denaturation of proteins causes major changes in original native form of proteins without altering their primary structures. It is well-known that the structure of a protein dictates its function.

Urea is a well-known denaturant shown to destabilize the native structure of a protein. Two mechanisms have been proposed to interpret the denaturation effect of urea, a direct and an indirect mechanism. Direct mechanism is when urea interacts with hydrophobic side chains, polar side chains or with the backbone. Indirect mechanism is when urea changes the water properties to a solvent which causes protein denaturation. It has been shown that van- der Waals interactions between the hydrophobic solute and solvent is more attractive in urea due to an enthalpic driving force[71],[72]. This is explained by the large dipole moments and the high polarizability of urea. Calorimetric studies revealed that adding a high concentration of urea, up to 2M, to globular proteins

decreases the enthalpic and the entropy of unfolded proteins, which in turn decreases the Gibbs free energy of unfolding proteins and promotes protein unfolding[73].

Guanidine-HCl is a widely used denaturant that destabilizes the native states of macromolecules. It is a chaotropic agent that disrupts a non-covalent forces such as Vander Waals interaction, hydrogen bonding and hydrophobic effects.
Experimental contributions from Carrie Moon in this chapter include gel electrophoresis, tryptophan fluorescence, and ELISA.

4.1.2 Fluorescence binding assay of 8-anilino-1-naphthalenesulfonic acid (ANS)

To monitor CRP unfolding after incubation with different denaturants, 1-Anilinonaphthalene-8-sulfonic Acid (ANS), a hydrophobic fluorescent probe was utilized. ANS has been used frequently in biochemistry and biophysics research to study protein folding and aggregation. ANS has polarity due to its negative charge on the sulphonated naphthalene group and due to the amide group electrons in the aniline ring that form hydrogen bonds with the proteins.

It also has hydrophobicity due to its aniline ring and naphthalene backbone. ANS aromatic rings help to stabilize its binding with apolar regions of proteins[74].

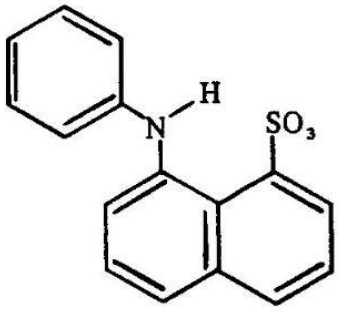

Figure 28. 1-Anilinonaphthalene-8-sulfonic Acid structure.

ANS binds to hydrophobic regions of protein noncovalently which leads to significant increase in quantum yield. The orientation of the two naphthyl groups of ANS becomes oriented in parallel upon binding to the

hydrophobic domains of the protein; this causes a significant increase in ANS intensity[75]. When the protein exposes more of its hydrophobic region, the binding events with ANS increase, which in turn causes an increase in the fluorescence intensity accompanied by blue shift. If the protein is fully denaturated, the ANS binding will become unstable and easily detach and become free in solution. Due to the loss of the organized structure of the fully denatured proteins, there is no longer a complimentary structure between the hydrophobic region and charged region, so ANS can just form one kind of interaction with the protein. In this case, the fluorescence intensity of ANS will become low as compared to partially denaturated proteins[74]. Possible fluorescence spectra of ANS is shown in

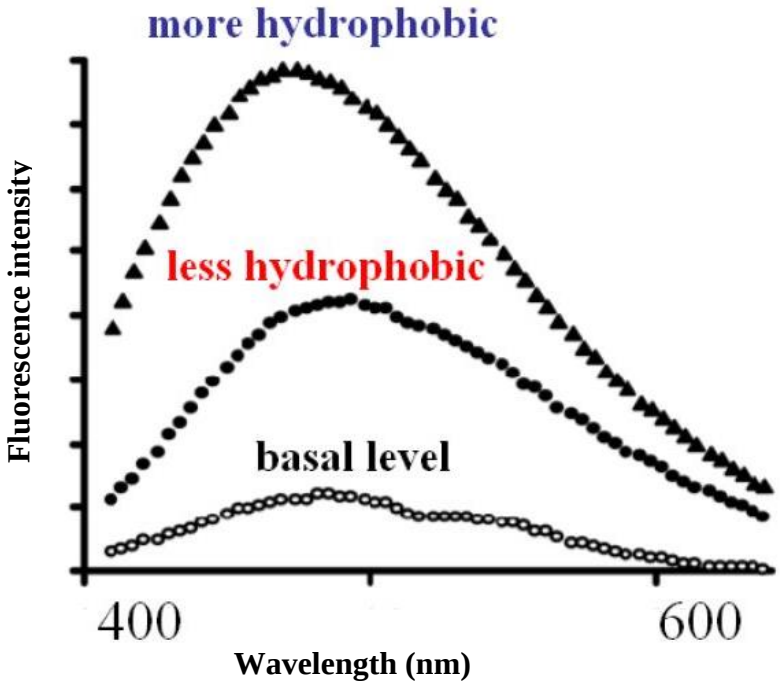

Figure 29. Possible ANS fluorescence spectra.
Possible ANS spectra upon its binding to protein's regions with different degree of hydrophobicity.

4.1.3 Tryptophan fluorescence assay

Tryptophan fluorescence is a widely used assay to monitor conformational changes of proteins. The maximum emission wavelength and the fluorescence intensity of tryptophan (Trp) are sensitive to the polarity of its local environment which makes it a good indicator for structural changes of proteins[76]. Trp fluorescence decreases and shifts to red with a longer wavelength when the Trp residue is exposed to an aqueous environment. pCRP contains 30 residues of Trp. The TRP residue location are 67, 100, 110, 162, 188, and 205 as shown in Figure 30. Inter subunit involves the 115-123 loop of one subunit and the 40-42 and 197-202 of adjacent protomer[7].

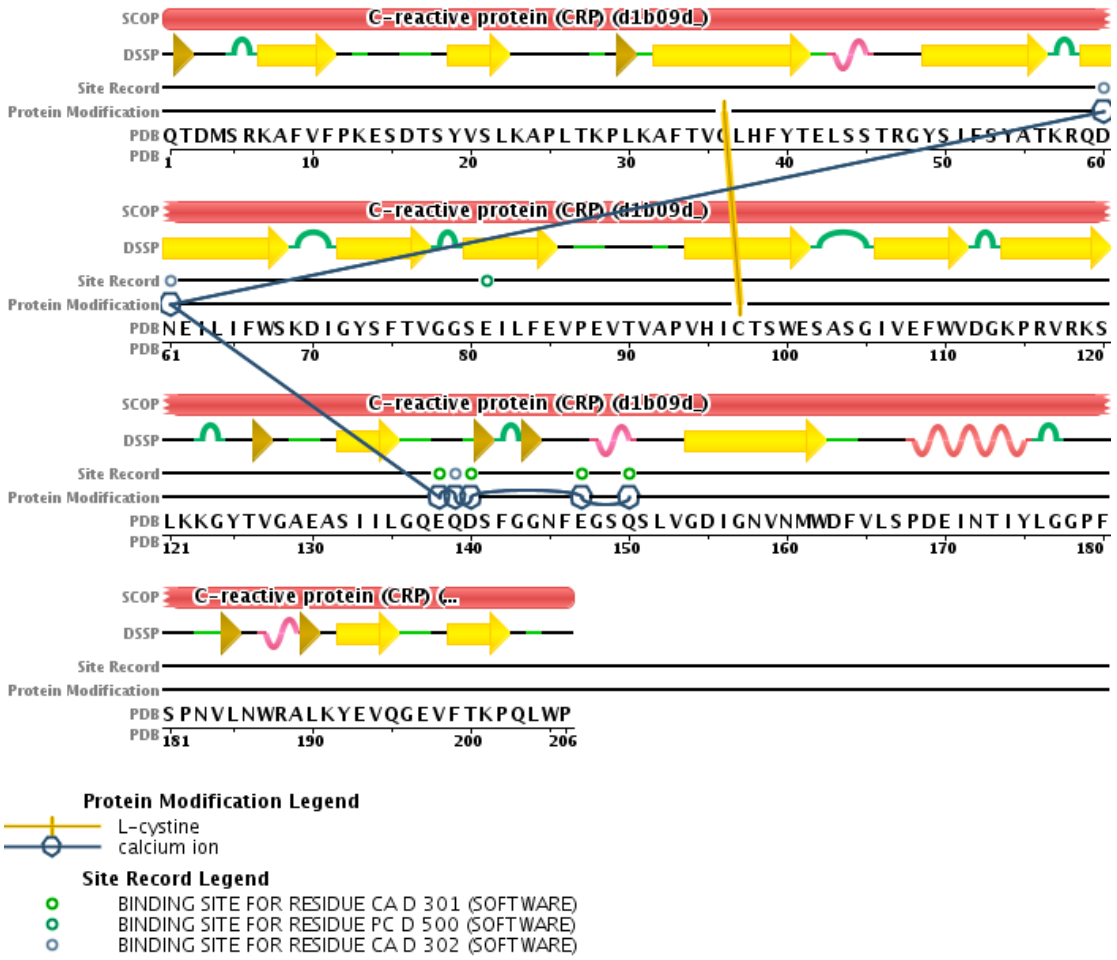

Figure 30. CRP amino acid sequence.
Tryptophans are found as residues 67, 100, 110, 162, 188, and 205.Image was taken from the protein data bank (PDB Identifier: 1B09).

4.2 Material and Methods

4.2.1 Modified Native PAGE

CRP forms were visualized using a modified Native Polyacrylamide Gel Electrophoresis system (PAGE)[42]. Standard Laemmli conditions were followed with the exception of using 0.005% SDS in the gel and using a native loading buffer (no SDS, BME, or heat). 0.43 μg of CRP was loaded in each well. Gels were run at 80 V for 2 hours and then silver stained. Bio-RAD precision plus protein standards ladder was used.

4.2.2 Tryptophan Fluorescence

Tryptophan Fluorescence of CRP was read using a Tecan Infinite M1000 plate reader with samples in Corning black half-area 96 well plates (product #3694). Measurements were made with an excitation wavelength of 280nm. The integral from the emission spectra from 300-400nm was used for comparing fluorescence intensity, and then each value was normalized to the average pCRP integrated intensity.

The standard buffer used in the experiments was 30 mM HEPES, 2 mM $CaCl_2$, 140 mM NaCl (chemicals purchased from Thermo-Fisher or Sigma Life Sciences unless otherwise noted). Purified human CRP (Academy Bio-medical Company #30P-CRP110) was used as pCRP when diluted with the standard buffer. CRP concentration per sample was 57.5 μg/mL. Each denaturant used for converting pCRP to mCRP was made in the standard buffer mentioned above. Stock solutions of 8 M urea, 10 mM EDTA and 6 M guanidine hydrochloride were made in the standard buffer and used for dilutions. Urea and guanidine CRP conversion trials were allowed to incubate for 2 hours at room

temperature prior to analysis. mCRP was also made with 0.01% SDS in standard buffer and heated for 1 hour at 80-85°C[42].

4.2.3 Binding assay of 1-Anilinonaphthalene-8-sulfonic Acid (ANS)

ANS, a hydrophobic fluorescent probe (Cayman chemical) was used to monitor the conformational changes of CRP after treating the protein with different denaturants. The stock solution of ANS was made using dimethyl sulfoxide (DMSO), and diluted to a final concentration of 200 μM by using Millipore water. Guanidine hydrochloride (2.5M, 5.7M), Urea-EDTA (3M, 6M) and HEPES buffer containing 2 mM $CaCl_2$, 140 mM NaCl with pH value 6.4 was used. CRP (50μg/ml) was incubated with the denaturants for 2 hours at 37°C.Then, ANS was added to the black polystyrol half area 96 well plate (Life Science). The fluorescence intensity of ANS was measured in a spectrofluorometer (Infinity M1000) by using an excitation wavelength of 390 nm, and an emission wavelength from 440 nm to 650nm. Tryptophan fluorescence measurements were also done before and after adding ANS to the plate.

4.3.3 Enzyme Linked Immunosorbent Assay (ELISA)

The binding of CRP to C1q was measured by performing an ELISA with C1q as a capture at a concentration of 1 μg/mL, following previously published procedures[42]. Bovine serum albumin (BSA, 1 μg/mL) was used as a control in place of the C1q capture. BSA and C1q were diluted in coating buffer (30 mM sodium carbonate, 70 mM sodium bicarbonate, pH 9.6, Sigma Aldrich). 100 μL of coating solution was added to the microwells in a Microlon 600 96W high binding clear microplate (Greiner Bioscience

655081). After a 2 hour incubation at 37 °C, wells were washed three times with 300 µL of phosphate buffered saline with 0.05% Tween-20 (PBST; Acros Organics) and once with 300 µL of phosphate buffered saline (PBS, pH 7.4). This was followed by tapping the plate dry on a stack of paper towels and Kimwipes. Next, 300 µL of blocking buffer (3% w/v BSA in PBST) was added and the plate was incubated at room temperature for 2 hours. In between each step in the assay, wells were washed as described above (300 µL in each well, 3 times with PBST and once with PBS) and then tapped dry on paper towels. 100 µL of CRP (1.8 µg/mL) in diluting buffer (1% w/v BSA in PBS) was added and incubated for 1 hour at 37 °C. The primary antibody, a biotinylated polyclonal anti-CRP was diluted at a ratio of 1:5,000 in diluting buffer and 100 µL was added and incubated for 1 hour at 37 °C. After washing, 100 µL of a 1:10,000 dilution of streptavidin-HRP (FROM?) was added to each well and incubated for 30 minutes at 37 °C. A final wash sequence was followed by the addition of 100 µL of 3, 3', 5, 5'-tetramethylbenzidine (TMB) substrate. After the color was allowed to develop (5-10 min) at room temperature, the reaction was stopped by the addition of 100 µL of 0.5 M sulfuric acid, turning the reaction solution from blue to yellow. Absorbance was measured at 450 nm, with a reference absorbance of 620 nm on a Microplate reader (Tecan infinite-M1000 PRO) plate reader.

4.3 Results and Discussion

4.3.1 Denaturing CRP reveals metastable states

To determine the stability of the native, pentameric form of CRP, we denatured CRP using two common denaturants, Urea with EDTA and GndHCl. The intrinsic, tryptophan fluorescence was measured and decreased with increasing denaturant, as expected, for most concentrations (Figure 31A and B). The change in fluorescence occurs as some of the 6 Trp residues (per monomer of CRP) go from a hydrophobic, protein environment to a more aqueous environment, where the fluorescence is substantially less. Denaturation with GndHCl led to a clear transition (Figure 31A) between 2.0 and 2.5 M GndHCl, however, the gradual decline in fluorescence from 0 to 2 M suggests conformational changes are occurring even at low concentration. CRP denatures quite easily but does not denature fully, as determine by comparing the fluorescence at 5M GndHCl to that of free Trp of the same concentration (Figure 30A).

After measuring the intrinsic fluorescence to identify changes in the exposure of Trp residues to aqueous environment, samples were loaded onto a native gel to assess the presence of different states of CRP. In Figure 31C, D, a clear transition occurs where a modified form of CRP begins to show up, running similar to the 20 kDa standard. pCRP is a 110 kDa pentamer with a pI at 6.4 and the pI changes to 5.6 upon monomerization[10]; both the molecular mass and the charge affect migration in this assay. The pentameric form is less charged and larger and therefore does not run well into the gel. With GndHCl treatment, this band first shows up at 1.75M GndHCl and is fully present at 2.75M, matching the profile of intrinsic fluorescence in Figure 30A.

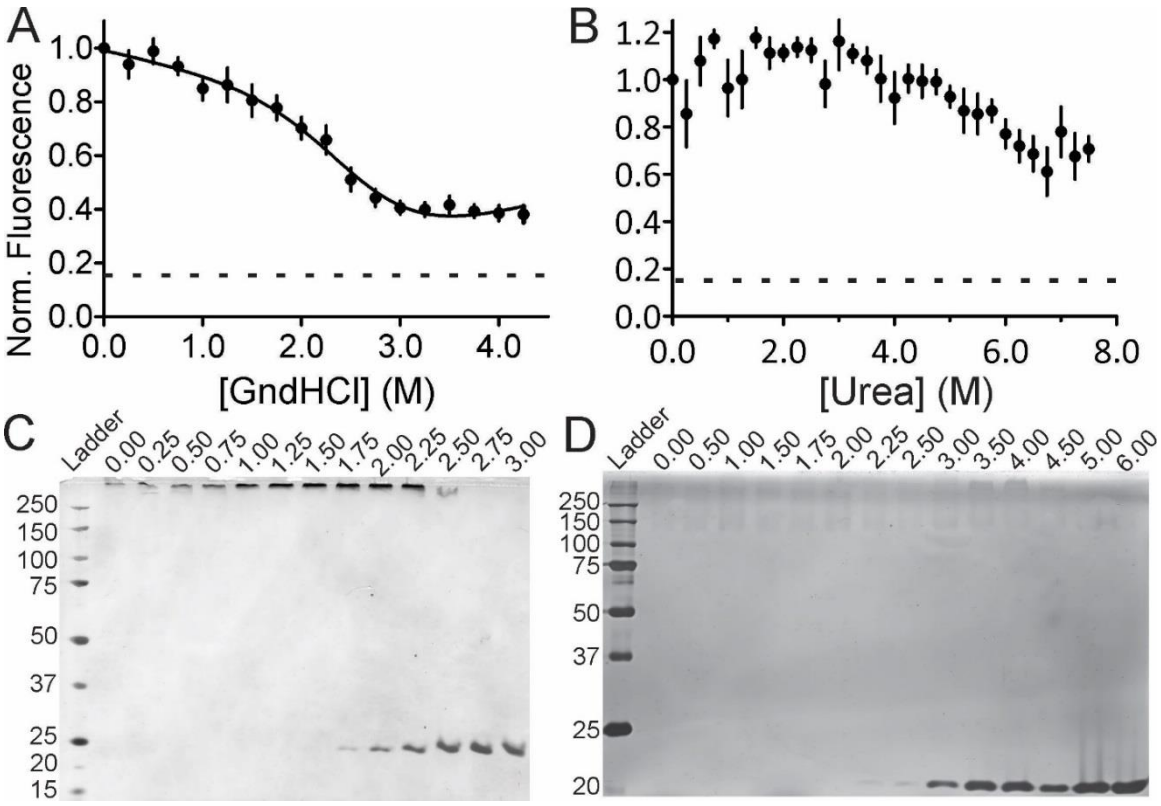

Figure 31. Intrinsic fluorescence and native PAGE assays of CRP treated with GndHCl and Urea.
Intrinsic, tryptophan fluorescence was measured by exciting solutions at 280 nm and recording fluorescence from 300-400 nm. The integrated fluorescence was normalized by the 0 M denaturant data point. Fluorescence decreased with increasing denaturants for both GndHCl (A) and Urea with EDTA (B). The dashed line in both represents the fluorescence intensity observed from an equivalent amount of free Trp. Error bars are +/- SEM. C) Native PAGE of GndHCl treated CRP with two hours of incubation, D) Native PAGE of Urea:EDTA treated CRP with two hours of incubation.

When pCRP is treated with Urea and EDTA, a clear transition exists in the gel from 2.25 to 4.0 M urea. The mCRP band increases over this range and the pCRP (not shown but retained in the stacking portion of the gel) disappears. A haze of protein is also observed in the gel and this fully disappears at 4.0M. This could be alternative states of pCRP that have not been fully characterized and these are present in the absence of Urea (Figure 31 D, 0M). The transition likely occurs over a larger range of urea concentrations

because urea is a weaker denaturant than GndHCl. Interestingly, the observed transition with Trp fluorescence is gradual from 2 – 6 M urea, over a much wider range than that observed in the gel, suggesting that conformational changes are still occurring that affect the Trp environment, but these changes do no broadly influence the size or charge of the protein in a way that affects how it runs on a gel.

4.3.2 Hydrophobic portions of CRP are exposed

To monitor CRP unfolding after incubation with different denaturants, 1-Anilinonaphthalene-8-sulfonic Acid (ANS), a hydrophobic fluorescent probe was utilized. ANS is used frequently in biochemistry and biophysics research to study protein folding and aggregation. ANS binds to hydrophobic regions of proteins, which leads to a significant increase in quantum yield and a blue shift in the emission maxima[74], [77]. As shown in Figure 32, treatment with 2.5M GndHCl (Figure 31A), 3 or 6 M urea (Figure 32B), or 0.01% SDS Figure 32C caused hydrophobic portions of CRP to be exposed. SDS-treated CRP showed the biggest change Figure 32 C, black circles from the untreated CRP (solid line in all figures). This means that more hydrophobic regions were exposed to ANS, and we suggested that this modified form of CRP (mCRP) mimics the physiological form of mCRP and maintain CRP function with downstream bindingTB partners as shown by another experiments performed in our lab.

Our data revealed an increase in ANS fluorescence intensity with a high degree of blue shift when CRP was treated with 2.5M of GndHCl or 3M of Urea-EDTA. This could be due to an increase in the degree of hydrophobicity which leads to a strong binding between ANS and CRP. However, a high concentration of the denaturants, 3M of

GndHCl and 6M of Urea-EDTA caused a decrease in ANS fluorescence intensity with low degree of blue shift Figure 32. At high concentration of GndHCl, ANS still retains high fluorescence. If a protein is completely unfolded, ANS does not bind. This agrees with Figure Figure 31A where Trp fluorescence remains despite high concentrations of GndHCl. Both demonstrate that CRP retains structure in high concentration of denaturant. CRP exposed to BME and heat showed less binding to ANS and less degree in blue shift Figure 32C as compared with CRP that treated with SDS. This reduce in ANS fluorescence could be attributed to the reducing effect of BME which disrupts the disulfide bond in the protein and leads to protein aggregation.

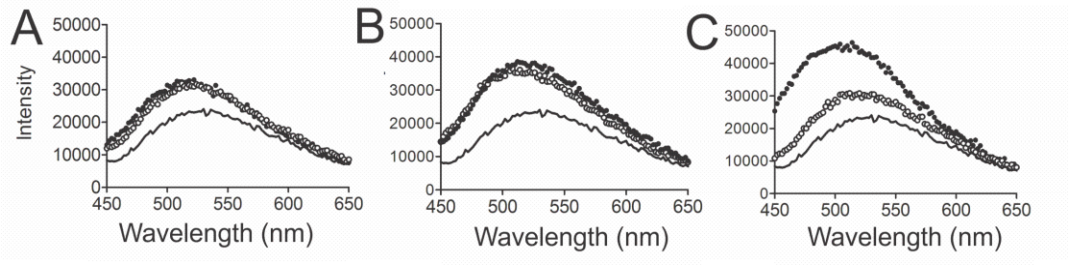

Figure 32. Treatment of pCRP with denaturants increase binding of 1-Anilinonaphthalene-8-sulphonic acid (ANS).
A) ANS fluorescence upon binding to pCRP incubated with 2.5 M GndHCl (filled circles) or 3.0 M GndHCl (open circles) for 2 hours at 37°C. B) ANS fluorescence upon binding to pCRP incubated with 3 M (open circles) and 6 M (filled circles) Urea-EDTA at 37°C for 2 hours. C) ANS fluorescence upon binding to pCRP that was incubated with 0.01% SDS and BME then heated at 100°C for one hour (open circles) or 0.01% SDS then heated at 80°C for one hour (filled circles). In all figures, ANS fluorescence when bound to pCRP without treatment is shown as a solid line.

4.4.4 SDS induced changes specifically increase C1q binding

In our lab we compared a variety of methods for synthesizing mCRP from serum purified pCRP, which were tested for the ability to produce a form that binds C1q, one downstream binding partner of CRP in the complement immune response. One of the methods for altering the conformation of pCRP is with 0.01% SDS and heat. ELISA experiments, performed by Carrie Moon, with C1q or BSA used to capture CRP were used to compare binding of different CRPs. A polyclonal antibody to CRP with a biotin linkage was used to then bind horseradish peroxidase linked streptavidin (HRP-Strep). In **Error! Reference source not found.**, the SDS treated CRP (blue) clearly shows significant binding to C1q as compared with pCRP (purple), or the antibody (green). The significant difference between mCRP and pCRP was confirmed with a Student's t-test p value of 0.0071 (unpaired, two-tailed). pCRP binding to C1q is similar to the antibody (green) which indicates that pCRP does not bind C1q measurably. When BSA is used as a capture, pCRP shows no significant binding (orange) as compared with C1q captures for pCRP (blue). BSA captures slightly more 0.01% SDS and heat treated CRP than pCRP (pink) or antibodies (yellow), but mCRP with C1q as a capture (blue) still shows the strongest binding. This data indicates that CRP treated with 0.01% SDS in 80°C for an hour produces a modified form that is biologically relevant to mCRP observed in vivo due to C1q binding. This agrees with the work of Wang et al[21], where fluorescence anisotropy revealed that SDS treated CRP binds C1q.

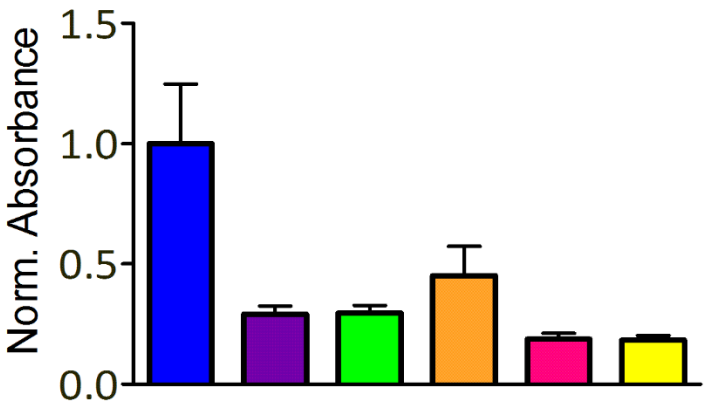

Capture	C1q	+	+	+	-	-	-
	BSA	-	-	-	+	+	+
Antigen	pCRP	-	+	-	-	+	-
	mCRP	+	-	-	+	-	-

Figure 33. Dilute SDS treated CRP binds C1q in an ELISA assay.
C1q or BSA was used as a capture agent for CRP. C1q captures CRP treated with 0.01% SDS and heated at 80°C for 1 hour (blue), but not pCRP (purple) or antibodies (green). BSA captures CRP significantly less than C1q (orange), but captures more 0.01% SDS: heat treated CRP than pCRP (pink) or antibodies (yellow). Error bars are +/- SEM and significance between mCRP and pCRP with C1q capture using an unpaired, two-tailed t-test is 0.0071.

.

4.4 Conclusion

In this work, we compared the unfolding of CRP using different chemical denaturants. We used Urea/EDTA, guanidine HCl, and 0.01% SDS with heat to perturb the pentameric state. All treatments give rise to a monomeric state in native PAGE experiments, but only dilute SDS with heat treatments maintain CRP function with downstream binding partners. Biological activity of the monomeric state was tested by a binding assay with C1q, a downstream binding partner of mCRP. This is consistent with what others have seen in past studies[21].

CHAPTER FIVE: SUMMARY

In this work, CRP binding and conversion was characterized as a function of membrane shape and chemical composition using a supported lipid bilayer biosensor that mimics the cell membrane. Despite knowing that the modified form of CRP, mCRP, binds downstream partners proteins better than the soluble form, pCRP, little is known about how these conformations affects CRP membrane interactions. The design of the biosensor permits to separately tune the lipids compositions and membrane shape. The primary component of lipids was POPC with and without lysoPC to mimic damaged membranes. The shape of membrane and curvature was controlled by using fluorescence nanoparticles with diameters (45 nm, 100 nm). Using this model system combined with quantitative fluorescence microscopy methods, CRP binding to lipid membranes was measured as a function of different conformations of CRP. The monomeric form of CRP bound curved membranes, but the pentameric form did not until membranes became highly curved (radius = 27 nm). Unlike most other curvature sensing proteins, mCRP accumulated at a higher density in lower curvatures. The presence of lysoPC increased binding of CRP to all membranes. Overall, our results show that the protein form, lipid composition, and membrane shape affect CRP interactions differently and the mechanism by which CRP recognizes damaged membranes depends on the combination of all three.

CRP interactions with cellular membranes was also investigated in this work using MES-SA cells. Valinomycin and Paclitaxel were used to induce apoptosis in MES-

SA cells. Apoptosis was confirmed using Annexin V, a protein binds to phosphatidylserine that exposed to the outer leaflet of the plasma membrane during the apoptosis. The data showed that CRP binds to the membrane of apoptotic cells more than the control cells.

Disassociation of CRP on the membrane of the apoptotic cells was then monitored by using a RNA-aptamer that binds specifically to mCRP. Cells incubated for two hours with mCRP bound aptamer significantly more than cells incubated for an hour. CRP incubated with apoptotic cells for two hours significantly bound aptamer more than CRP incubated for an hour. These results suggested that during two hours of incubation more pCRP disassociates to mCRP.

Unfolding of CRP was also characterized in this work using different chemical denaturants. Urea/EDTA, guanidine HCl, 0.01% SDS, and heat were used to perturb the pentameric state. All treatments give rise to a monomeric state in native PAGE experiments. The change in conformation was also assessed by tryptophan and ANS fluorescence. ANS binds to hydrophobic regions of proteins, which leads to a significant increase in quantum yield and a blue shift in the emission maxima. ANS fluorescence intensity increased when CRP treated with 2.5M Gnd-HCl, and with 3M urea-EDTA suggested that more hydrophobic regions were exposed and bound to ANS. The effect of different pH on CRP conformation was also assessed using ANS.

This work could lead to a more specific diagnostic test for CVD risk based on CRP conformers and provide a new direction for atherosclerosis treatment.

REFERENCES

[1] M. M. Ewing, "Post-interventional atherosclerotic vascular remodeling preclinical investigation into immune modulatory therapies," Leiden University, 2013.

[2] D. Thompson, M. B. Pepys, and S. P. Wood, "The physiological structure of human C-reactive protein and its complex with phosphocholine," *Structure*, vol. 7, no. 2, pp. 169–177, 1999.

[3] S. D. de Ferranti and N. Rifai, "C-reactive protein: a nontraditional serum marker of cardiovascular risk," *Cardiovasc. Pathol.*, vol. 16, no. 1, pp. 14–21, 2007.

[4] L. Marnell, C. Mold, and T. W. Du Clos, "C-reactive protein: Ligands, receptors and role in inflammation," *Clin. Immunol.*, vol. 117, no. 2, pp. 104–111, 2005.

[5] S. Verma and E. T. H. Yeh, "C-reactive protein and atherothrombosis--beyond a biomarker: an actual partaker of lesion formation.," *Am. J. Physiol. Regul. Integr. Comp. Physiol.*, vol. 285, no. 5, pp. R1253–R1256; discussion R1257–R1258, 2003.

[6] S. U. Eisenhardt, J. Habersberger, A. Murphy, Y. C. Chen, K. J. Woollard, N. Bassler, H. Qian, C. Von Zur Muhlen, C. E. Hagemeyer, I. Ahrens, J. Chin-Dusting, A. Bobik, and K. Peter, "Dissociation of pentameric to monomeric C-reactive protein on activated platelets localizes inflammation to atherosclerotic plaques," *Circ. Res.*, vol. 105, no. 2, pp. 128–137, 2009.

[7] J. Volanakis, "Human C-reactive protein: expression, structure, and function," *Mol. Immunol.*, vol. 38, pp. 189–197, 2001.

[8] M. Fujita, Y. K. Takada, Y. Izumiya, and Y. Takada, "The binding of monomeric C-reactive protein (mCRP) to Integrins αvβ3 and α4β1 is related to its pro-inflammatory action.," *PLoS One*, vol. 9, no. 4, p. e93738, 2014.

[9] A. Bíró, Z. Rovó, D. Papp, L. Cervenak, L. Varga, G. Füst, N. M. Thielens, G. J. Arlaud, and Z. Prohászka, "Studies on the interactions between C-reactive protein and complement proteins," *Immunology*, vol. 121, no. 1, pp. 40–50, 2007.

[10] L. a Potempa, B. a Maldonado, P. Laurent, E. S. Zemel, and H. Gewurz, "Antigenic, electrophoretic and binding alterations of human C-reactive protein modified selectively in the absence of calcium.," *Mol. Immunol.*, vol. 20, no. 11, pp. 1165–1175, 1983.

[11] S. Devaraj, U. Singh, and I. Jialal, "The evolving role of C-reactive protein in atherothrombosis," *Clin. Chem.*, vol. 55, no. 2, pp. 229–238, 2009.

[12] C. Mold, S. Nakayama, T. J. Holzer, H. Gewurz, and T. W. Du Clos, "C-reactive protein is protective against Streptococcus pneumoniae infection in mice.," *J. Exp. Med.*, vol. 154, no. 5, pp. 1703–1708, 1981.

[13] M.-K. Chang, C. J. Binder, M. Torzewski, and J. L. Witztum, "C-reactive protein binds to both oxidized LDL and apoptotic cells through recognition of a common ligand: Phosphorylcholine of oxidized phospholipids.," *Proc. Natl. Acad. Sci. U. S. A.*, vol. 99, no. 20, pp. 13043–13048, 2002.

[14] N. H. H. Heegaard and F. A. Robey, "A capillary electrophoresis-based assay for the binding of Ca2+ and phosphorylcholine to human C-reactive protein," *J. Immunol. Methods*, vol. 166, no. 1, pp. 103–110, 1993.

[15] P. Munder and M. Modolell, "Lysophosphatidylcholine (lysolecithin) and its synthetic analogues. Immunemodulating and other biologic effects," *Springer Semin. ...*, vol. 203, pp. 187–203, 1979.

[16] D. Balleza, "Mechanical properties of lipid bilayers and regulation of mechanosensitive function: from biological to biomimetic channels.," *Channels (Austin).*, vol. 6, no. 4, pp. 220–233, 2012.

[17] J. R. Henriksen, T. L. Andresen, L. N. Feldborg, L. Duelund, and J. H. Ipsen, "Understanding detergent effects on lipid membranes: A model study of lysolipids," *Biophys. J.*, vol. 98, no. 10, pp. 2199–2205, 2010.

[18] John E Volanakis, "Interaction of C-reactive protein with artifical bilayers," *Nature*, vol. 281, pp. 155–157, 1979.

[19] S.-R. Ji, Y. Wu, L. Zhu, L. a Potempa, F.-L. Sheng, W. Lu, and J. Zhao, "Cell membranes and liposomes dissociate C-reactive protein (CRP) to form a new, biologically active structural intermediate: mCRP(m).," *FASEB J.*, vol. 21, no. 1, pp. 284–294, 2007.

[20] S. L. Hazen, "Oxidized phospholipids as endogenous pattern recognition ligands in innate immunity," *J. Biol. Chem.*, vol. 283, no. 23, pp. 15527–15531, 2008.

[21] M. S. Wang, R. E. Messersmith, and S. M. Reed, "Membrane curvature recognition by C-reactive protein using lipoprotein mimics," *Soft Matter*, vol. 8, no. 30, p. 7909, 2012.

[22] H. W. Wang and S. F. Sui, "Dissociation and subunit rearrangement of membrane-bound human C-reactive proteins.," *Biochem. Biophys. Res. Commun.*, vol. 288, no. 1, pp. 75–79, 2001.

[23] T. Khreiss, L. József, L. a. Potempa, and J. G. Filep, "Conformational Rearrangement in C-Reactive Protein Is Required for Proinflammatory Actions on Human Endothelial Cells," *Circulation*, vol. 109, no. 16, pp. 2016–2022, 2004.

[24] D. J. Hammond, S. K. Singh, J. a. Thompson, B. W. Beeler, A. E. Rusiñol, M. K. Pangburn, L. a. Potempa, and A. Agrawal, "Identification of acidic pH-dependent ligands of pentameric C-reactive protein," *J. Biol. Chem.*, vol. 285, no. 46, pp. 36235–36244, 2010.

[25] S. Taskinen, P. T. Kovanen, H. Jarva, S. Meri, and M. O. Pentikäinen, "(1) Taskinen, S.; Kovanen, P. T.; Jarva, H.; Meri, S.; Pentikäinen, M. O. Biochem. J. 2002, 367 (2), 403–412.Binding of C-reactive protein to modified low-density-lipoprotein particles: identification of cholesterol as a novel ligand for C-reactive protei," *Biochem. J.*, vol. 367, no. 2, pp. 403–412, 2002.

[26] T. P. Zwaka, V. Hombach, and J. Torzewski, "C-reactive protein-mediated low density lipoprotein uptake by macrophages: implications for atherosclerosis.," *Circulation*, vol. 103, no. 9, pp. 1194–1197, 2001.

[27] A. J. Nauta, L. a. Trouw, M. R. Daha, O. Tijsma, R. Nieuwland, W. J. Schwaeble, A. R. Gingras, A. Mantovani, E. C. Hack, and A. Roos, "Direct binding of C1q to apoptotic cells and cell blebs induces complement activation," *Eur. J. Immunol.*,

vol. 32, no. 6, pp. 1726–1736, 2002.

[28] H. Païdassi, P. Tacnet-Delorme, V. Garlatti, C. Darnault, B. Ghebrehiwet, C. Gaboriaud, G. J. Arlaud, and P. Frachet, "C1q binds phosphatidylserine and likely acts as a multiligand-bridging molecule in apoptotic cell recognition.," *J. Immunol.*, vol. 180, no. 4, pp. 2329–2338, 2008.

[29] a Agrawal, a K. Shrive, T. J. Greenhough, and J. E. Volanakis, "Topology and structure of the C1q-binding site on C-reactive protein.," *J. Immunol.*, vol. 166, no. 6, pp. 3998–4004, 2001.

[30] M. Chang, K. Hartvigsen, J. Ryu, Y. Kim, and K. H. Han, "The pro-atherogenic effects of macrophages are reduced upon formation of a complex between C-reactive protein and lysophosphatidylcholine," pp. 1–10, 2012.

[31] E. Gregory J. Hardya, Rahul Nayaka, S. Munir Alamb, Joseph G. Shapterc, Frank Heinrichd and and S. Zauschera, "Biomimetic supported lipid bilayers with high cholesterol content formed by á-helical peptide-induced vesicle fusion," *J Mater Chem*, vol. 22, no. 37, pp. 19506–19513, 2012.

[32] "https://avantilipids.com/product/840072/," *Avanti Polar Lipids, Inc. 700 Industrial Park Drive Alabaster, Alabama 35007-9105*. .

[33] joshua C. Black, "Development of a biosensor for investigating membrane curvature sorting," University of Denver.

[34] H. T. Mcmahon and J. L. Gallop, "Membrane curvature and mechanisms of dynamic cell membrane remodelling," vol. 438, no. December, 2005.

[35] J. C. Black, P. P. Cheney, T. Campbell, and M. K. Knowles, "Membrane curvature based lipid sorting using a nanoparticle patterned substrate.," *Soft Matter*, vol. 10, no. 12, pp. 2016–23, 2014.

[36] J. Crocker, J. Crocker, and D. Grier, "Methods of Digital Video Microscopy for Colloidal Studies," *J. Colloid Interface Sci.*, vol. 179, no. 1, pp. 298–310, 1996.

[37] D. Blair and E. Dufresne, "The Matlab Particle Tracking Code Repository." [Online]. Available: http://site.physics.georgetown.edu/matlab/. [Accessed: 10-

Jun-2014].

[38] B. T. Larson, K. a Sochacki, J. M. Kindem, J. W. Taraska, and S. L. Schmid, "Systematic spatial mapping of proteins at exocytic and endocytic structures.," *Mol. Biol. Cell*, vol. 25, no. 13, pp. 2084–93, 2014.

[39] S. Barg, M. K. Knowles, X. Chen, M. Midorikawa, and W. Almers, "Syntaxin clusters assemble reversibly at sites of secretory granules in live cells.," *Proc. Natl. Acad. Sci. U. S. A.*, vol. 107, no. 48, pp. 20804–9, 2010.

[40] A. L. Mattheyses, S. M. Simon, and J. Z. Rappoport, "Imaging with total internal reflection fluorescence microscopy for the cell biologist.," *J. Cell Sci.*, vol. 123, no. Pt 21, pp. 3621–3628, 2010.

[41] D. Axelrod, D. E. Koppel, J. Schlessinger, E. Elson, and W. W. Webb, "Mobility measurement by analysis of fluorescence photobleaching recovery kinetics," *Biophys. J.*, vol. 16, no. 9, pp. 1055–1069, 1976.

[42] M. S. Wang, J. C. Black, M. K. Knowles, and S. M. Reed, "C-reactive protein (CRP) aptamer binds to monomeric but not pentameric form of CRP," *Anal. Bioanal. Chem.*, vol. 401, no. 4, pp. 1309–1318, 2011.

[43] J. E. Volanakis and a J. Narkates, "Interaction of C-reactive protein with artificial phosphatidylcholine bilayers and complement.," *Journal of immunology (Baltimore, Md. : 1950)*, vol. 126, no. 5. pp. 1820–1825, 1981.

[44] B. Y. I. Kushner, A. Melvin, and H. K. An, "STUDIES OF ACUTE PHASE PROTEIN I. AN I~UNOltlSTOCHEMICAL METHOD FOR "rHa~ LOCALIZATION OF Cx-REACTIVE PROTEIN IN RABBITS. ASSOCIATION WITH NECROSIS IN LOCAL INFLAMMATORY LESIONS," *exp.Med*, vol. 114, pp. 961–974, 1962.

[45] P. L. Yeagle, W. C. Hutton, C. Huang, and R. B. Martin, "Phospholipid head-group conformations; intermolecular interactions and cholesterol effects.," *Biochemistry*, vol. 16, no. 20, pp. 4344–4349, 1977.

[46] T. Goda, Y. Miyahara, A. Chemie, A. Chemie, K. L. Madsen, V. K. Bhatia, U. Gether, and D. Stamou, "BAR domains, amphipathic helices and membrane-anchored proteins use the same mechanism to sense membrane curvature," *Acta*

Biomater., vol. 40, no. 9, pp. 1848–1855, 2015.

[47] R. M. Heuertz, G. P. Schneider, L. A. Potempa, and R. O. Webster, "Native and modified C-reactive protein bind different receptors on human neutrophils," *Int. J. Biochem. Cell Biol.*, vol. 37, no. 2, pp. 320–335, 2005.

[48] A. J. Narkates and J. E. Volanakis, "C-reactive protein binding specificities: artificial and natural phospholipid bilayers.," *Ann. N. Y. Acad. Sci.*, vol. 389, pp. 172–82, 1982.

[49] B. J. Peter, "BAR Domains as Sensors of Membrane Curvature: The Amphiphysin BAR Structure," *Science (80-.).*, vol. 303, no. 5657, pp. 495–499, 2004.

[50] V. K. Bhatia, K. L. Madsen, P.-Y. Bolinger, A. Kunding, P. Hedegård, U. Gether, and D. Stamou, "Amphipathic motifs in BAR domains are essential for membrane curvature sensing.," *EMBO J.*, vol. 28, no. 21, pp. 3303–3314, 2009.

[51] S. Vanni, L. Vamparys, R. Gautier, G. Drin, C. Etchebest, P. F. J. Fuchs, and B. Antonny, "Amphipathic lipid packing sensor motifs: Probing bilayer defects with hydrophobic residues," *Biophys. J.*, vol. 104, no. 3, pp. 575–584, 2013.

[52] N. S. Hatzakis, V. K. Bhatia, J. Larsen, K. L. Madsen, P.-Y. Bolinger, A. H. Kunding, J. Castillo, U. Gether, P. Hedegård, and D. Stamou, "How curved membranes recruit amphipathic helices and protein anchoring motifs.," *Nature chemical biology*, vol. 5, no. 11. pp. 835–841, 2009.

[53] M. Mammen, "Polyvalent interaction in biological systems: Implications for Design and use of Multivalent Ligands and Inhibitors," vol. 37, no. 20, pp. 2754–2794, 1998.

[54] T. Goda and Y. Miyahara, "Engineered zwitterionic phosphorylcholine monolayers for elucidating multivalent binding kinetics of C-reactive protein," *Acta Biomater.*, 2015.

[55] T. Goda and Y. Miyahara, "Engineered zwitterionic phosphorylcholine monolayers for elucidating multivalent binding kinetics of C-reactive protein," *Acta Biomater.*, vol. 40, pp. 46–53, 2015.

[56] D. Gershov, S. Kim, N. Brot, and K. B. Elkon, “C-Reactive protein binds to apoptotic cells, protects the cells from assembly of the terminal complement components, and sustains an antiinflammatory innate immune response: implications for systemic autoimmunity.,” *J. Exp. Med.*, vol. 192, no. 9, pp. 1353–1364, 2000.

[57] T. W. Du Clos, “Pentraxins : Structure , Function , and Role in Inflammation,” vol. 2013, 2013.

[58] G. Mariño and G. Kroemer, “Mechanisms of apoptotic phosphatidylserine exposure.,” *Cell Res.*, vol. 23, no. 11, pp. 1247–8, 2013.

[59] Y. Kikuchi, “High-affinity RNA aptamers to C-reactive protein (CRP): newly developed pre-elution methods for aptamer selection.”

[60] S. Elmore, “Apoptosis: A Review Of Programmed Cell Death,” *Changes*, vol. 53, no. 4, p. 495–, 200AD.

[61] A. Rev, P. Mech, D. Downloaded, K. L. Rock, and H. Kono, “The Inflammatory Response to Cell Death,” *Annual Reivew of Pathology: Mechanisms of Disease*, vol. 3. pp. 99–126, 2008.

[62] Z. Darwich, A. S. Klymchenko, O. A. Kucherak, L. Richert, and Y. M??ly, “Detection of apoptosis through the lipid order of the outer plasma membrane leaflet,” *Biochim. Biophys. Acta - Biomembr.*, vol. 1818, no. 12, pp. 3048–3054, 2012.

[63] K. Kholmurodov, “Molecular dynamics simulations of valinomycin interactions with potassium and sodium ions in water solvent,” *Adv. Biosci. Biotechnol.*, vol. 01, no. 03, pp. 216–223, 2010.

[64] I. J. Furlong, C. Lopez Mediavilla, R. Ascaso, A. Lopez Rivas, and M. K. Collins, “Induction of apoptosis by valinomycin: mitochondrial permeability transition causes intracellular acidification,” *Cell Death Differ.*, vol. 5, no. 3, pp. 214–221, 1998.

[65] P. B. Schiff and S. B. Horwitz, “Taxol stabilizes microtubules in mouse fibroblast cells.,” *Proc. Natl. Acad. Sci. U. S. A.*, vol. 77, no. 3, pp. 1561–5, 1980.

[66] S. S. Bacus, a V Gudkov, M. Lowe, L. Lyass, Y. Yung, a P. Komarov, K. Keyomarsi, Y. Yarden, and R. Seger, "Taxol-induced apoptosis depends on MAP kinase pathways (ERK and p38) and is independent of p53.," *Oncogene*, vol. 20, no. 2, pp. 147–155, 2001.

[67] S. Cagnol and J.-C. Chambard, "ERK and cell death: Mechanisms of ERK-induced cell death - apoptosis, autophagy and senescence," *FEBS J.*, vol. 277, no. 1, pp. 2–21, 2010.

[68] S.-R. Ji, L. Ma, C.-J. Bai, J.-M. Shi, H.-Y. Li, L. a Potempa, J. G. Filep, J. Zhao, and Y. Wu, "Monomeric C-reactive protein activates endothelial cells via interaction with lipid raft microdomains.," *FASEB J.*, vol. 23, no. 6, pp. 1806–1816, 2009.

[69] M. Mihlan, a. M. Blom, K. Kupreishvili, N. Lauer, K. Stelzner, F. Bergstrom, H. W. M. Niessen, and P. F. Zipfel, "Monomeric C-reactive protein modulates classic complement activation on necrotic cells," *FASEB J.*, vol. 25, no. 12, pp. 4198–4210, 2011.

[70] B. S. Cummings, L. P. Wills, and R. G. Schnellmann, "Measurement of Cell Death in Mammalian Cells," *Curr Protoc Phamacol*, vol. 1, no. Lemasters 1999, pp. 1–30, 2004.

[71] Matteus Lindgren, *On the Mechanism of Urea-Induced Protein Denaturation*, vol. 93, no. 2. 2010.

[72] B. J. Bennion and V. Daggett, "The molecular basis for the chemical denaturation of proteins by urea.," *Proc. Natl. Acad. Sci. U. S. A.*, vol. 100, no. 9, pp. 5142–7, 2003.

[73] M. I. P. A. Z. Andrade, M. N. Jones, and H. A. Skinner, "The Enthalpy of Interaction of Urea with Some Globular Proteins," vol. 131, pp. 127–131, 1976.

[74] M. Biology and P. Health, "1-anilinonaphthalene-8-sulfonate (ANS); a versatile fluorescent probe from protein folding study to drug design," vol. 12, no. 6, pp. 1–12, 2010.

[75] A. Chapeaurouge, J. S. Johansson, and S. T. Ferreira, "Folding of a de novo designed native-like four-helix bundle protein," *J. Biol. Chem.*, vol. 277, no. 19,

pp. 16478–16483, 2002.

[76] J. T. Vivian and P. R. Callis, “Mechanisms of tryptophan fluorescence shifts in proteins.,” *Biophys. J.*, vol. 80, no. 5, pp. 2093–2109, 2001.

[77] E. Schonbrunn, S. Eschenburg, K. Luger, W. Kabsch, and N. Amrhein, “Structural basis for the interaction of the fluorescence probe 8-anilino-1-naphthalene sulfonate (ANS) with the antibiotic target MurA.,” *Proc. Natl. Acad. Sci. U. S. A.*, vol. 97, no. 12, pp. 6345–6349, 2000.

APPENDIX

Supplemental Figures

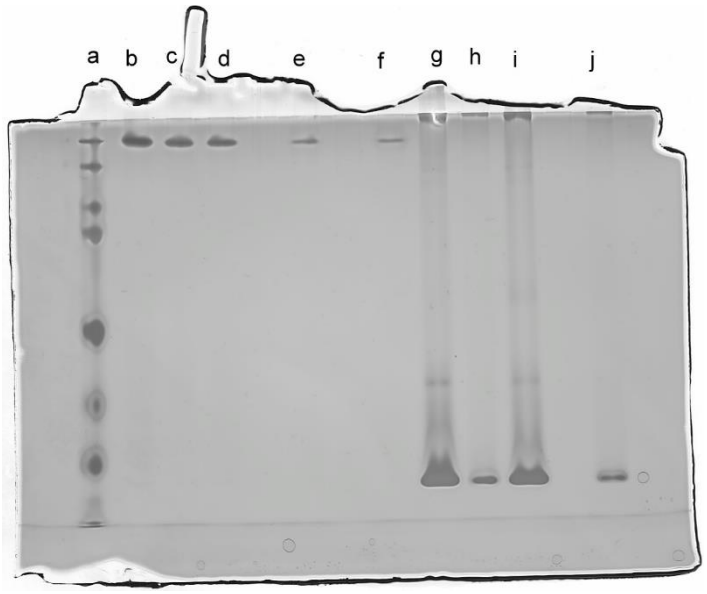

S 1. Native PAGE of pCRP, mCRP in HEPES, and PIPES buffer.
a- Ladder. b,c- 50ug/ml of pCRP in HEPES, and PIPES respectively. d,e- 40ug/ml of pCRP in HEPES, and PIPES respectively. f- 30ug/ml of pCRP in PIPES. g,i- mCRP made by heating pCRP with 0.01%SDS at 80c for an hour and left overnight before loaded to gel. h, and j- fresh mCRP.

S 2. Dot blot of primary anti- C-reactive protein (C6), mouse IgG monoclonal-antibody, and secondary goat anti mouse immunoglobulin G with Alexa 488.

S 3. Dot blot of primary anti- C-reactive protein (D7), mouse IgG monoclonal-antibody, and secondary goat anti mouse immunoglobulin G with Alexa 488.This has been done twice and it is qualitatively the same with mCRP less intense than pCRP.

Disassociation constant for the interaction of CRP with different ligands as determined by surface plasmon resonance

	K_d
CRP-Phosphorylcholine	18 µM
pCRP-pCRP	23 µM
pCRP-C1q	1.45 nM
mCRP-C1q	0.28 nM

Matlab Codes used for these experiments

CALCCORF CODE by Dr. Michelle Knowles

```
function out=calccorf (red, green)

% CALL: out=calccorf(red, green);
%
% PURPOSE:  to measure the Pearson's correlation coefficient between pairs of cropped
images.
% INPUT:
% red: a ministack of croppped images that are stable in time (red NPs,
% granules, clathrin pits, etc)
% green: a ministack of cropped images that are more variable (syx,
% proteins) - this is the channel that intensity is measured for.

nredrows = length(red(1,1,:));
ngrnrows = length(green(1,1,:));
nrows = min(nredrows, ngrnrows);

msk = zeros([1,2]);

for i = 1:nrows;
   g = green(:,:,i);
   r = red(:,:,i);
   normg = double(g)/double(max(max(g)));
   normr = double(r)/double(max(max(r)));
% calculate the Pearson's correlation coefficent (code from Taraska).
   msk (i,1) = corr2(normr, normg);
% remove saturated images DOES NOT WORK
%    if max(max(g)) OR max(max(r)) = 4095 then
%       msk (i, 2) = NaN
   msk (i,2) = corr2(normg, normr);

end
mean(msk)
out = msk;
end
```

RUN_MINISTK CODE modified by Mitch Alton

```
function [] = run_ministk ( )

%ask for red and green channels
[redfile,redpth] = uigetfile('*.tif','Select the Red Channel');
[grnfile,grnpth] = uigetfile('*.tif','Select the Green Channel');

%ask where to save the resulting file
[savefile,savepth] = uiputfile('*.mat','Where to save the Results');

%read in an image
a=imread([redpth,redfile]);
c=imread([grnpth,grnfile]);

%view the image, imagesc autoscales.
colormap('gray'),imagesc(a);

% filter the image, 9 is a size, filter things larger than 9 pixels, and filter 1 or smaller
b=bpass(a, 1, 9);
colormap('gray'),imagesc(b);
colormap('gray'),image(b);
%seems to make a saturated mask like image when using beads

%use the filtered image to find regions. 1500 is the threshold and 9 is a size of feature
%you are looking for. Should be the same as above. RECORD THESE NUMBERS IN
%YOUR NOTEBOOK!
pk=pkfnd(b, 100, 9);

%find centroids -  NOT NEEDED for colocalization routine
cnt=cntrd(b, pk, 15);

%overlay regions onto non-filtered image. Adjust the threshold to find fewer or more
%spots.
colormap('gray'),imagesc(a);
hold on
plot(pk(:,1), pk(:,2), 'ro');
zoom

%once you like the threshold and want to cut out ministacks
%do this with both color channels so that you can check it.
cutout_red = ministk(a, pk, 24, 9);
cutout_grn = ministk(c, pk, 24, 9);

%a is the image you will be cropping, pk are the regions you would like to crop, 24 (+1)
```

```
%is the size of images you will cut out and if spots are too close (within 9 pixels of one
%another) you will not count either of them.

%save the file
stkwrite(cutout_red,strcat(savefile,'-red.stk'),savepth);
stkwrite(cutout_grn,strcat(savefile,'-grn.stk'),savepth);

cutout_red_avg = uint16(mean(cutout_red,3));
cutout_grn_avg = uint16(mean(cutout_grn,3));

stkwrite(cutout_red_avg,strcat(savefile,'-red-avg.stk'),savepth);
stkwrite(cutout_grn_avg,strcat(savefile,'-grn-avg.stk'),savepth);

%see what regions were kept and save them. You do NOT need to do this with both
%image files, since the spot locations will be identical.
finalspt = keptspot(a, pk, 24, 9);
save(fullfile(savepth,savefile));

% you can view what spots were kept and what were ?too close? to others or the edges.

colormap('gray'),imagesc(a);
hold on
plot(finalspt(:,1), finalspt(:,2), 'ro');
zoom

%% Make a radial plot of pixel intensity
% This is Mitch Alton's implementation

hold off;

[m, n]=size(cutout_grn_avg);

%finds size of the image
x=[1:n];
l=repmat(x,n,1);

%creates matrix of repeating columns of 1 through how ever many columns
%there are in the image
y=[1:m];
y';
p=repmat(y,m,1);
w=p';

%creates matrix of repeating rows
x=l-(((n-1)*0.5)+1);
```

```
y=w-(((n-1)*0.5)+1);

%makes matrixes -# to +#. Not sure how this will work with even numbers
%though
z=cutout_grn_avg(1:m,1:n);

%creates a matrix of intensities from image
[THETA,RHO,Z]=cart2pol(x,y,z);

%converts three matrixes to a three dimentional polar coordinate matrix
%G=reshape(z,1,625);
%H=reshape(RHO,1,625);

%turns matrix into a list of values
[t,I,J] = unique(RHO);
s = zeros(size(t));
frequencies = zeros(size(t));
for i = 1:max(J)
   I = find(J==i);
   s(i) = mean(Z(I));
   frequencies(i) = length(I);
end
plot(t,s)

% Save the files
radialPlot = cat(2,t,s);
hgexport(gcf, fullfile(grnpth,[savefile '-grn-radial.png']), hgexport('factorystyle'),
'Format', 'png');
csvwrite(fullfile(grnpth,[savefile '-grn-radial.csv']), radialPlot);



[m, n]=size(cutout_red_avg);

%finds size of the image
x=[1:n];
l=repmat(x,n,1);

%creates matrix of repeating columns of 1 through however many columns
%there are in the image
y=[1:m];
y';
p=repmat(y,m,1);
w=p';
```

```
%creates matrix of repeating rows
x=l-(((n-1)*0.5)+1);
y=w-(((n-1)*0.5)+1);

%makes matrixes -# to +#. Not sure how this will work with even numbers
%though
z=cutout_red_avg(1:m,1:n);

%creates a matrix of intensities from image
[THETA,RHO,Z]=cart2pol(x,y,z);

%converts three matrixes to a three dimentional polar coordinate matrix
%G=reshape(z,1,625);
%H=reshape(RHO,1,625);

%turns matrix into a list of values
[t,I,J] = unique(RHO);
s = zeros(size(t));
frequencies = zeros(size(t));
for i = 1:max(J)
   I = find(J==i);
   s(i) = mean(Z(I));
   frequencies(i) = length(I);
end
plot(t,s)

% Save the files
radialPlot = cat(2,t,s);
hgexport(gcf, fullfile(grnpth,[savefile '-red-radial.png']), hgexport('factorystyle'),
'Format', 'png');
csvwrite(fullfile(grnpth,[savefile '-red-radial.csv']), radialPlot);

%close
end
```

```
function out=ministk(im,rgn,sz,sepdist)
% out=ministk(im,rgn,sz)
%
% PURPOSE:  to cut out small regions of an image based on spots found in
% the image or a corresponding image of a different color. This is used to
% measure colocalization based on the work of Knowles and Barg in two PNAS
% 2011 papers. Spots are found using the work of tracking routines
% available on Eric Weeks' website (Emory University) and made into Matlab
% by Eric Dufrense.
% INPUT:
% im: image to cut from
% rgn: spots (x,y) about which regions should be cut
% sz: size of cut out (a square of sz by sz pixels)
% sepdist: is the minimum separation distance between two spots. If two
% spots are within this distance of one another, neither are counted.
%
% OUTPUT:  a sz x sz x N image array
%
% CREATED: Michelle Knowles May 2012

%if sz/2 == floor(sz/2)
%warning('sz must be even so that the spots can be centered on a pixel: 1 pixel added');
%sz = sz+1
%end

%scott's code for a mask
pix=(sz+1)/2;
dim = length(im);
nrgn = length(rgn(:,1));


%create a blank image array that you can fill
msk=zeros([sz+1,sz+1]);
%loop through all regions that locate spots in an image
for i =1:nrgn;
   x = rgn(i,1);
   y = rgn(i,2);
   %don't include regions within pix distance from the edge of the image.
   if ((x>pix) & ((x+pix)<dim) & (y>pix) & ((y+pix)<dim))
      % don't include regions within "sepdist" pixels of another region
      % calculate an array that contains the difference between the
      % current particle's postion and all others.
```

```
      diffy=rgn(:,2)-rgn(i,2);
      diffx=rgn(:,1)-rgn(i,1);
      mag=((diffx.*diffx)+(diffy.*diffy).^0.5);
      % find all the locations in the magnitude array that are non-zero.
      % This should remove the comparison between particle i and itself,
      % which will always be zero.
      w = find(mag);
      mag = mag(w);
      if (min(mag) > sepdist)
        cutout = imcrop(im,[x-pix y-pix sz sz]);
        msk = cat(3, msk, cutout);
      end
    end
end

out=msk;
end
```

```
%better_colo plots intensities of a location guided average image as a
%function of distance from the center of the image. The second hald of the
%program finds the area under the peak of the radial intensity plot. It
%does this by dividing by the mean of the data after
%the third pixel.
%Written by Mitch Alton on 7/15/15
[m, n]=size(a);
%finds size of the image
x=[1:n];
l=repmat(x,n,1);
%creates matrix of repeating columns of 1 through however many columns
%there are in the image
y=[1:m];
y';
p=repmat(y,m,1);
w=p';
%creates matrix of repeating rows
x=l-(((n-1)*0.5)+1);
y=w-(((n-1)*0.5)+1);
%makes matrixes -# to +#. Not sure how this will work with even numbers
%though
z=a(1:m,1:n);
%creates a matrix of intensities from image
[THETA,RHO,Z]=cart2pol(x,y,z);
%converts three matrixes to a three dimentional polar coordinate matrix
G=reshape(z,1,(m*n));
H=reshape(RHO,1,(m*n));
%turns matrix into a list of values
[t,I,J] = unique(H);
s = zeros(size(t));
frequencies = zeros(size(t));
for i = 1:max(J)
   I = find(J==i);
   s(i) = mean(G(I));
   frequencies(i) = length(I);
end
%this averages the intensities (Z) for single distance (RHO) values
ydatatemp=s(:,8:83);
%limits the yvalues to just the values past 3 pixels from the center of the
%image. The nanoparticle seems to only be 3 pixels in radius.
base=mean(ydatatemp);
```

```
%finds the average of all of the data past the 3rd pixel for the height of
%the rectangle
yaxis=s/base;
ypeak=yaxis(:,1:7);
plot(t,yaxis)
clear sum
x=sum(ypeak);
answer=x-1
%this gives a number for the area of the peak from the colocalization
%as the answer
```

SPOTTEST CODE by Dr. Philip Cheney

```
%spottest -- Load, look for spots, show a picture
%
% this program is used to determine the properties of a movie or image
% containing spots.
%
% INPUT:
%   movieOrImage is a movie or image containing spots
%
%
% PC 24 Apr 2014
%
% This is converted from the old spot check functions, so there may be
% unused cruft still hanging around in here.

figure;
movieOrImageLoaded = loadSingleTIFF(movieOrImage);
sawSpots = seeingSpotsAml(movieOrImageLoaded,1);

imshow(movieOrImageLoaded(:,:,1),[min(movieOrImageLoaded(:))
max(movieOrImageLoaded(:))*0.5]);
hold on;
plot(sawSpots.spotsDetected(:,1,1),sawSpots.spotsDetected(:,2,1),'ro','MarkerSize',20);
title('Frame 1');

if eq(sawSpots.isMovie,1)
   figure;
   sawSpots = seeingSpotsAml(movieOrImageLoaded,sawSpots.numberFrames);

imshow(movieOrImageLoaded(:,:,sawSpots.numberFrames),[min(movieOrImageLoaded
(:)) max(movieOrImageLoaded(:))*0.5]);
   hold on;
   plot(sawSpots.spotsDetected(:,1,1),sawSpots.spotsDetected(:,2,1),'ro','MarkerSize',20);
   title(['Frame ',num2str(sawSpots.numberFrames)]);
end
```